Journal of Medicinal Chemistry Article

J. Med. Chem. **2010,** *53,* 1741–1754 **1741**
DOI: 10.1021/jm901652p

Discovery and Optimization of Novel 3-Piperazinylcoumarin Antagonist of Chemokine-like Factor 1 with Oral Antiasthma Activity in Mice

Gang Li,[†] Dongmei Wang,[†] Mingna Sun, Guangyan Li, Jinfeng Hu, Yun Zhang, Yuhe Yuan, Haijie Ji, Naihong Chen,* and Gang Liu*

Institute of Materia Medica, Chinese Academy of Medical Sciences and Peking Union Medical College, 2 Nanwei Rd, Beijing 100050, P. R. China.
[†]*These authors contributed equally to this work.*

Received November 9, 2009

Chemokine-like factor 1 (CKLF1) is a novel functional cytokine that acts through its receptor CC chemokine receptor 4 (CCR4). Activation of CCR4 by CKLF1 plays an important role in diseases such as asthma and multiple sclerosis. This article describes a cell-based screening assay using an FITC-labeled CCR4 agonist (CKLF1-C27), a CKLF1 peptide fragment. Screening of our in-stock small-molecule library identified a 3-piperazinylcoumarin analogue **1** ($IC_{50} = 4.36 \times 10^{-6}$ M) that led to the discovery of orally active compound **41** ($IC_{50} = 2.12 \times 10^{-8}$ M) through systematic optimization. Compound **41** blocked the calcium mobilization and chemotaxis induced by CKLF1-C27 and reduced the asthmatic pathologic changes in lung tissue of human CKLF1-transfected mice. Further studies indicated that compound **41** ameliorated pathological changes via inhibition of the NF-κB signal pathway.

Introduction

Chemokines are the secreted basic proteins of 8−10 kDa that represent the largest family of cytokines encoded in the human genome.[1] Chemokines exert their effects through seven transmembrane G-protein-coupled receptors. To date, over 50 chemokines have been identified, and 17 chemokine receptors have been described in humans. Chemokines can be grouped tentatively into four subfamilies according to their structural criteria, particularly the position of a pair of cysteines located at or near the N-terminus of each protein.[2] Most chemokines are members of the CC or CXC class, where the two N-terminal cysteines are adjacent or have a single amino acid separating them, respectively.[3] Another C-class feature of the single N-terminal cysteine in which the two cysteines are separated by three residues, termed the CX3C class, has also been described.[4]

Chemokines were originally identified by their ability to regulate the trafficking of immune cells.[5−7] Through their interaction with G-protein-coupled receptors on target cell surfaces, chemokines initiate a serial signaling cascade. The biological role of chemokines extends beyond their ability to function as chemoattractants. They have since been shown to be involved in many other biological processes,[8] including growth regulation,[9] hematopoiesis,[10−12] and angiogenesis.[13,14] Many diseases and conditions have been related to the dysregulation of chemokine networks, such as rheumatoid arthritis (RA),[15] osteoarthritis,[16] multiple sclerosis,[17] atherosclerosis,[18] Alzheimer's disease,[19] and asthma.[20] This relationship provides a strong rationale for targeting chemokines and chemokine receptors in developing new drugs.[21]

Chemokine-like factor 1 (CKLF1[a]), part of the human chemokine-like factor superfamily, is a human cytokine that was isolated from phytohemagglutinin (PHA) stimulated U937 cells.[22] CKLF1 maps to chromosome 16q 22.1, which has three other isoforms (CKLF2, CKLF3, and CKLF4), all of which share the conserved N-terminal and C-terminal ends. CKLF1 has a CC motif, and the key amino acids around this motif are identical to those of macrophage-derived chemokine (MDC) and thymus and activation regulated chemokine (TARC), although the latter lacks the additional two C-terminal cysteines. Similar to the functions of MDC and TARC, CKLF1 exhibits potential chemotactic activity in a wide spectrum of leukocytes both in vitro and in vivo.[22] CKLF1 is expressed widely in human tissues, especially in the lung and peripheral blood leukocytes. CKLF1 stimulates the proliferation of murine skeletal muscle cells after in vivo administration of naked CKLF1 and promotes the proliferation of rat aortic smooth muscle cells.[23] CKLF1 plasmid transformation causes a pathological change in somniferous tubules in rats, leading to infertility.[24] CKLF1 has been reported to have significant chemotactic effects on human arterial smooth muscle cells because CKLF1-induced chemotaxis was blocked by pertussis toxin (PTX) at 10 μg, L^{-1}.[23]

CKLF1 is also associated with autoimmune diseases such as RA and asthma. In the asthmatic rat, CKLF1 gene expression in the lungs is significantly higher in asthmatic

*To whom correspondence should be addressed. For N.C.: phone, 86-10-63165177; fax, 86-10-63165177; e-mail, chennh@imm.ac.cn. For G.L.: phone, 86-10-63167165; fax: 86-10-63165246; e-mail: gliu@imm.ac.cn.

[a] Abbreviations: CKLF1, chemokine-like factor 1; CCR4, CC chemokine receptor 4; FITC, fluorescein isothiocyanate; PTX, pertussis toxin; PBMCs, peripheral blood mononuclear cells; MDC, macrophage-derived chemokine; HEK293, human embryonic kidney 293; TARC, thymus and activation regulated chemokine; HRP, horseradish peroxidase; Th2, T helper 2; WBC, white blood cell; EOS, eosinophil; DEX, dexamethasone; NF-κB, nuclear factor-κB; IκB, inhibitor of nuclear factor-κB; IKK, inhibitor of nuclear factor-κB kinase; HTS, high-throughput screening; IC_{50}, concentration for 50% inhibition.

Published on Web 01/25/2010

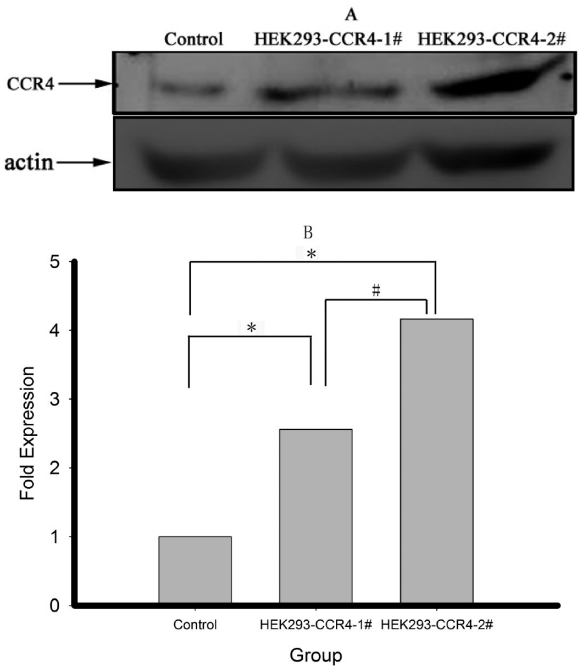

Figure 1. Measurement of CCR4 by Western blotting. (A) two monoclonal HEK293-CCR4 cell lines 1# and 2# were identified by anti-CCR4 polyclonal IgG. (B) The density of each band was quantified by image analysis. The expression of CCR4 was significantly higher in HEK293-CCR4 2# than in HEK293-CCR4 1# cells: (*) $p < 0.01$ vs control, (#) $p < 0.05$, HEK293-CCR4 1# vs HEK293-CCR4 2#. All experiments were repeated at least three times, and representative data are shown.

animals than in controls. The level of CKLF1 mRNA is higher in peripheral blood mononuclear cells from asthmatic patients than in healthy donors. The expression of CKLF1 is up-regulated during the asthma process.[25] A single intramuscular injection of CKLF1 plasmid DNA into BALB/c mice causes dramatic pathological changes in the lungs of treated mice. These changes included peribronchial leukocyte infiltration, epithelial shedding, collagen deposition, proliferation of bronchial smooth muscle cells, and fibrosis of the lung, which are similar to those observed in chronic persistent asthma and acute respiratory distress syndrome.[26]

The functional receptor of CKLF1 is CCR4.[27] The CKLF1 binding motif to CCR4 has been characterized as a 27-amino acid residual peptide (ALIYRKLLFNPSGPYQKKPVHEKKEVL, CKLF1-C27).[28] CCR4 is expressed preferentially on T helper 2 (Th2) cells, and CCR4-expressing cells have been described at sites of allergic inflammation. CCR4 also plays an essential role in the recruitment of Th2 cells into the airway upon allergen stimulation.[29−31] Interrupting the recruitment of allergen-specific Th2 cells is viewed as a highly attractive potential therapeutic strategy for allergic disease.[32] This suggests that interruption of the CCR4-CKLF1−ligand axis is a potential therapeutic strategy for allergic airways disease such as allergic asthma. However, none of the small-molecule antagonists of the CCR4-CKLF1 interaction has been reported yet.

In this article, we describe our development of a competition binding assay using FITC-labeled CKLF1-27 as a ligand. A novel 3-piperazinylcoumarin analogue **41** is identified as a potent antagonist through evaluation both in vitro and in mice. We first clarify that the lesion induced by the CKLF1 plasmid was related to the overactivation of the nuclear factor-κB (NF-κB) signaling pathway and that **41** can regulate the abnormal activation of the NF-κB signaling pathway in mice.

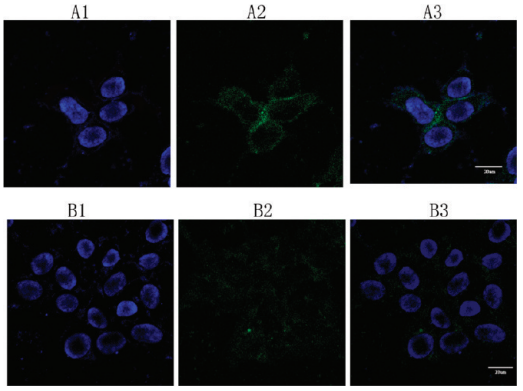

Figure 2. Confocal laser scanning microscopy was used to map the expression of CCR4 in HEK293-CCR4 2# cells. These images were taken from fixed cells. The receptor was localized using anti-CCR4 antibody and FITC-labeled goat antirabbit antibody. All experiments were repeated at least twice, and representative data are shown (bar = 20 μm). Parts A1 and B1 were stained by Hoechst 33458. A2, B2 were labeled with anti-CCR4 antibody and FITC-labeled goat antirabbit antibody. Part A3 overlaps with parts A1 and A2, and part B3 overlaps with parts B1 and B2.

Results and Discussion

Development of a High-Throughput Screening Assay. HEK293-CCR4 cells are stable recombinant HEK293 cells that overexpress the human CCR4 receptor.[28] Lipofectamine 2000 was used to select the monoclonal cell lines expressing higher levels of CCR4 protein. The HEK293 cells were transfected by human pCDI-CCR4 according to the manufacturer's instructions, selected by G418, and amplified. Two cell lines were obtained and coded as HEK293-CCR4 1# and 2# (Figure 1). The cells were harvested, and CCR4 expression was analyzed by Western blotting. The expression of CCR4 was 1.6-fold higher in the HEK293-CCR4 2# cells than in the HEK293-CCR4 1# cells. The distribution of CCR4 protein in HEK293-CCR4 2# cells was localized by confocal microscopy; the CCR4 protein was marked using anti-CCR4 polyclonal antibody (human IgG) and subsequent FITC-labeled goat antirabbit IgG. The cell nucleus was stained by Hoechst 33458. CCR4 was highly expressed on the cell membrane of HEK293-CCR4 2# cells (parts A1, A2, and A3 of Figure 2) but not in the mock HEK293 cells (parts B1, B2, and B3 of Figure 2).

The CKLF1-C27 was used as the mimic of CKLF-1 binding to CCR4. The overall advantages by using small molecule peptide to develop an assay are its easy synthesis and high quality and quantity available, which are necessary for high throughput screening. The screening conditions such as the concentration of FITC-CKLF1-C27, cell count, and the coculture time were then optimized (Figure 3). The final screening conditions were defined as 0.08 μM of FITC-CKLF1-C27 (Figure 3A), 6×10^3 cells/well of HEK293-CCR4 2# (Figure 3B), and 50 min of coculture (Figure 3C).

Discovery of the Antagonists of the CKLF1−CCR4 Interaction Using the New Assay and Analysis of the Structure−Activity Relationships (SARs). To identify the transactional antagonists of CKLF1 and CCR4, over 2000 unrelated compounds in our stocked library as the source of structural diversity were screened using the ligand−receptor competition

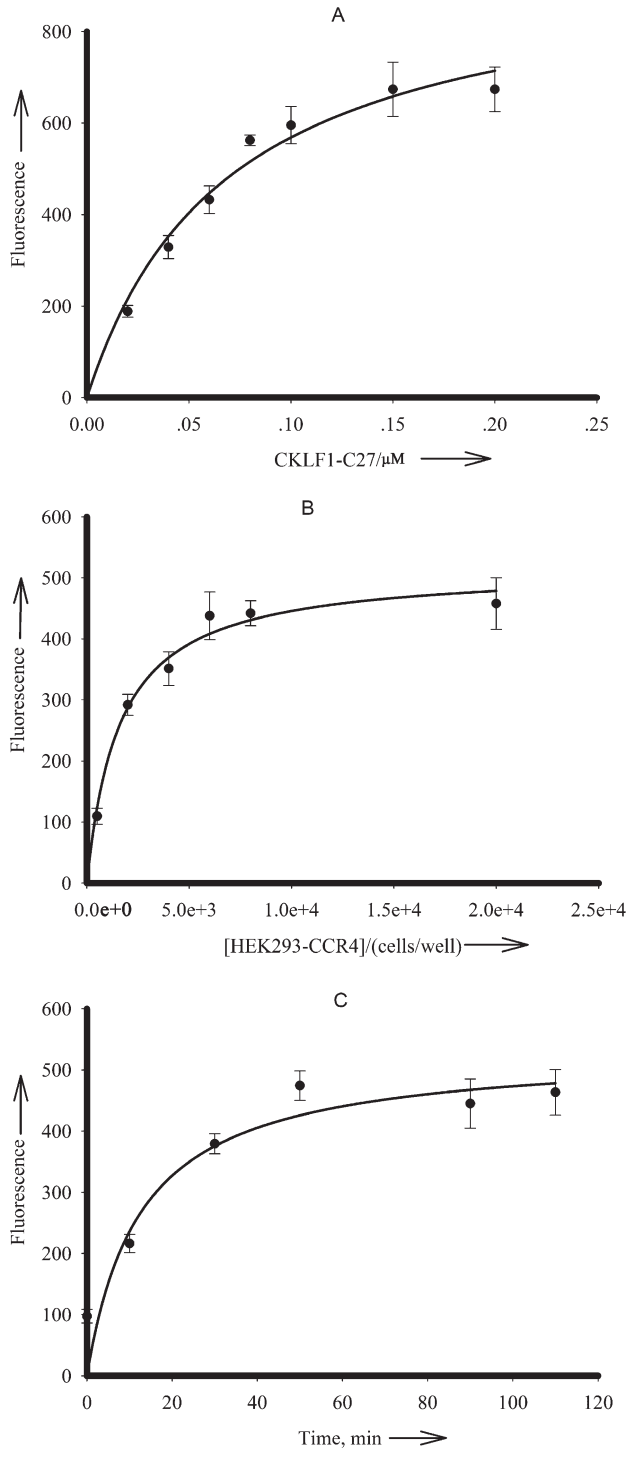

Figure 3. A high-throughput screening assay was established. (A.) The FITC-CKLF1-C27 concentration correlated with fluorescence release. The cell count and the coculture time were set at 8×10^3 cell/well and 60 min, respectively. When the concentration of FITC-CKLF1-C27 was 0.08 μM, the fluorescence release was sensitive mainly to exogenous compound. (B) The HEK293-CCR4 2# cell count giving the maximum fluorescence was 6×10^3 cells with 0.08 μM FITC-CKLF1-C27 and 60 min coculture. (C) Fluorescence release was maximum at 50 min of coculture with 6×10^3 HEK293-CCR4 2# cells per cell count and 0.08 μM FITC-CKLF1-C27. ($n = 16$).

binding assay.[43] The initial search gave two classes of compounds that exhibited promising inhibitory activity by about 35% and 57% at an initial tested compound concentration of 10 μM (Figure 4).

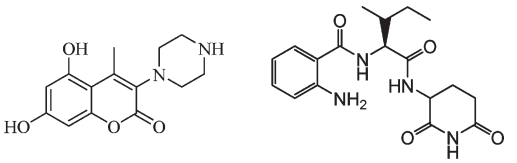

1 $IC_{50}=4.36\times10^{-6}$M **2** $IC_{50}=8.36\times10^{-4}$M

Figure 4. The two antagonists identified in the initial screening.

Table 1. Coumarin Analogues and Their Inhibitory Percentage (%) at 10 μM

Compd	Structure	Inhibition	Compd	Structure	Inhibition
4	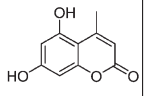	32.28%	13	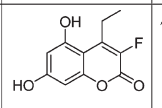	7.55%
5	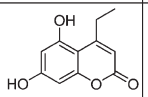	23.58%	14	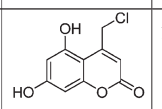	1.07%
6	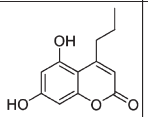	1.18%	15	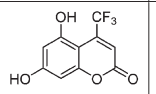	2.66%
7	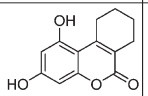	39. 85%	16	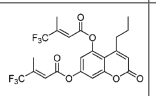	1.37%
8	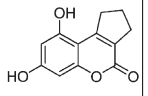	35.19%	17	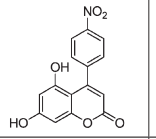	9.84%
9	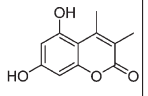	20.28%	18	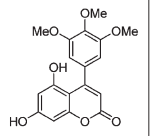	3.85%
10	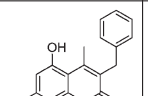	20.48%	19	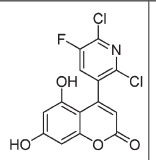	9.44%
11	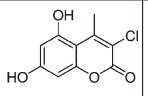	2.80%	20	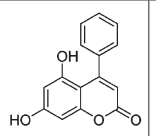	18.62%
12	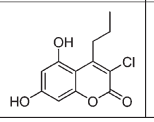	1.36%			

With this encouraging result, a second round of screening was performed to outline the preliminary SARs bearing a common structural feature of coumarin pharmacophore in our library (Table 1). The activities of all 17 coumarin analogues selected showed that the piperazine group of compound **1** at the C3-position of coumarin contributed a key feature required for a high level of inhibitory potency. A look at the preliminary SARs gave the structural information

of other substituents and positions. Halogen groups at the C3- or C4-position significantly reduced the active potency (< 10%) or inactivated it completely (**11**, **12**, **13**, **14**, and **15**). Aromatic replacements at the C3- or C4-position were also useless (**10**, **17**, **18**, **19**, and **20**). 5,7-Dihydroxyl groups could not be blocked simultaneously (**16**). The length of carbon chain at the C4-position affected the inhibitory potency. Elongation reduced its activity (**4**, **5**, and **6**); however, a cycloalkane at the C3 and C4 positions did not significantly decrease the inhibitory percentage at 10 μM (**7**, **8**).

To confirm further the importance of the piperazine substituent at the C3-position, three close analogues of compound **1** were designed and synthesized in which the piperazine ring was replaced by a morpholinyl (**21**), piperadinyl (**22**), or phenyl (**23**) ring. Reaction of 3-chloro-4-methylcoumarin **11** with morpholine or piperidine in pyridine afforded **21** or **22**, respectively (Scheme 1). Compound **23** was prepared using a base-catalyzed Kostanecki condensation of 2,4,6-trihydroxylacetophenone and phenylacetyl chloride in the presence of anhydrous Cs_2CO_3 (Scheme 2). Compounds **21**, **22**, and **23** proved to be completely inactive, further suggesting that the piperadinyl group at the C3-position is crucial for maintaining the activity (data not shown).

On the basis of these preliminary SARs, we conclude that the novel 3-piperazinylcoumarin is a basic structural feature for its antagonistic activity that interrupts the CCR4−CKLF1 interaction. A focused sublibrary was then designed, synthesized, and evaluated (Chart 1).

Because 3-piperazinylcoumarin is a new pharmacophore, one challenge is to predict the most desirable substitution to induce an antagonistic profile of the CCR4-CKLF1 interaction. To explore the influence of substituents at the NH group of C3-piperazinecoumarin,

Chart 1. 3-Piperazinylcoumarin Template

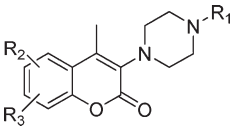

Scheme 1. Synthetic Route of the Target Compounds **21** and **22**[a]

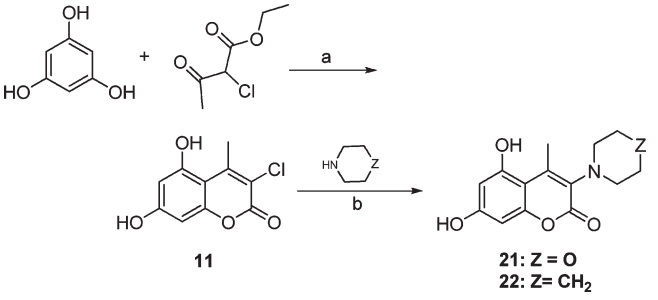

[a] Reagents and conditions: (a) HCl/CH_3OH; (b) pyridine, reflux.

Scheme 2. Synthesis of Compound **23**[a]

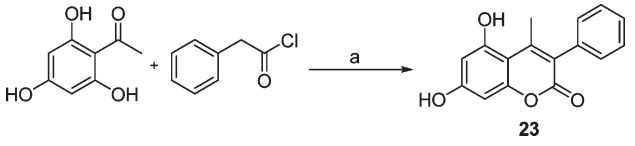

[a] Reagents and conditions: (a) Cs_2CO_3, acetone.

Table 2. Acylations of **1** at the NH Group of C3-Piperazinecoumarin and Their Inhibitory Potency

Compd	Structure	IC_{50}	Compd	Structure	IC_{50}
24	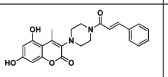	1.57×10^{-6}	30	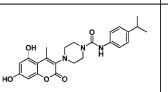	1.32×10^{-6}
25	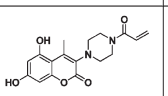	4.24×10^{-6}	31	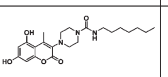	5.39×10^{-7}
26	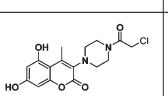	8.58×10^{-5}	32	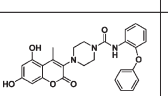	6.00×10^{-6}
27	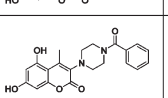	4.36×10^{-6}	33	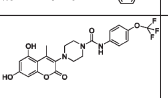	1.10×10^{-7}
28	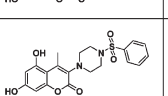	6.04×10^{-6}	34	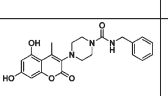	1.59×10^{-6}
29	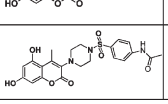	2.56×10^{-6}			

Scheme 3. Synthetic Route of the Target Compounds **24**−**34**[a]

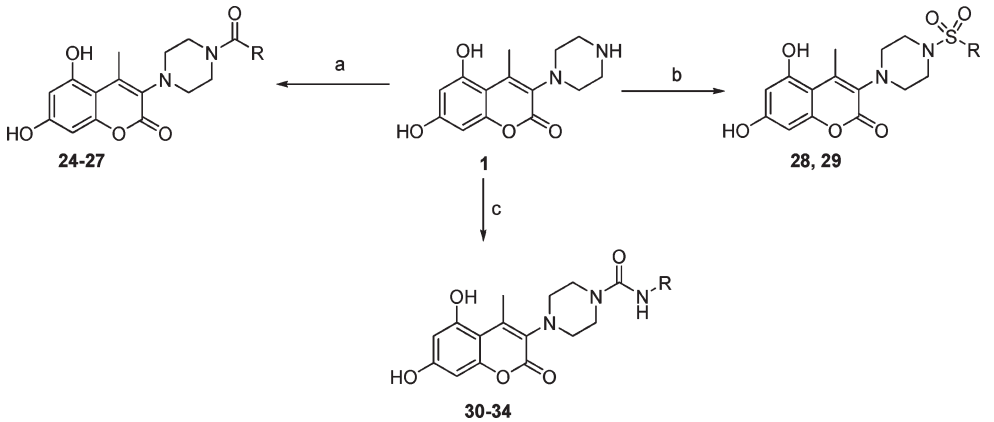

[a] Reagents and conditions: (a) RCOCl, Et_3N, THF/DMF, 45 °C; (b) RSO_2Cl, pyridine, THF/DMF, 60 °C ; (c) RNCO, THF/DMF, 50 °C.

compound **1** was first reacted with various chloride acyls, including electron-withdrawing and electron-donating groups. This produced compounds **24**−**27** (Table 2) in the presence of Et_3N. Compounds **28** and **29** were alternatively synthesized by sulfonation of **1** with chloride sulfone, whereas compounds **30**−**34** were prepared by reaction of **1** with isocyanates in THF aided by DMF (Scheme 3).

The results of the competition binding assay are presented in Table 2. Eight compounds (**24**, **25**, **27**−**30**, **32**, **34**) showed nearly equivalent activity with **1** at a micromolar level of the IC_{50} value. However, **31** and **33**, which were incorporated into a urea pharmacophore, had the best inhibitory potency by an increase of almost 1 log.

Alkyl or lyophobic aryl groups were introduced into the NH of piperazine, as seen in compounds **41**−**47** (Table 3). The reaction of 2-chloro-β-ketoester with various commercially available piperazine derivatives in the presence of anhydrous K_2CO_3 gave the corresponding intermediates (**35**−**40**), followed by a Pechmann condensation with 2,4,6-trihydroxylbenzene to afford the anticipated compounds **41**−**46** (Scheme 4). Compound **47** was prepared by a reductive alkylation of NH of **1** and 2-ethylbutanal in the presence of $NaBH_3CN$ (Scheme 5).

The subsequent competition binding assay indicated that **41** ($IC_{50} = 2.12 \times 10^{-8}$ M) with methyl substitution gave the highest inhibitory potency; however, compound **47** with bulk alkane substituents did not show measurable activity (Table 3). Direct aromation of the NH of piperazine (**43**−**46**) also resulted in a loss of activity.

Finally, the role of 5,7-dihydroxyl groups was examined. Compounds **49**−**54** were prepared by the method used to prepare compound **41** (Scheme 6). Treatment of 2-chloro-β-ketoester with *N*-methylpiperazine in the presence of anhydrous K_2CO_3 gained the intermediate **48**, which was subsequently allowed to react with commercially available substituted phenols, providing compounds **49**−**54**. Compounds **55**−**62** were prepared through a Mitsunobu reaction of **49** with the appropriate alcohols in the presence of DEAD and PPh_3, (Scheme 7). Removing the 5-hydroxyl group did not change the potency much (**49**) in vitro (Table 4). The rest of the compounds, in which one or two 5,7-dihydroxyl groups were replaced with variable substituents, exhibited at least 10 times decrease in potency to **41**. This result indicates that the 5,7-hydroxyl groups were contributable.

Table 3. Reductive Alkylations of the NH Group of **1** and Their Inhibitory Potency

Compd	Structure	IC_{50}	Compd	Structure	IC_{50}
41	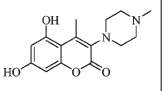	2.12×10^{-8}	45	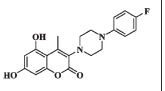	5.85×10^{-5}
42	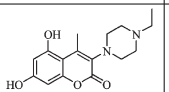	1.31×10^{-7}	46	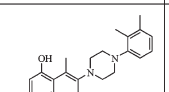	3.13×10^{-5}
43	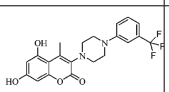	1.51×10^{-5}	47	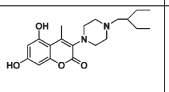	>10μM
44	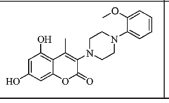	>10μM			

Alternative Cellular Activity of Compound 41. To test compound **41** in vitro further, two functional assays of calcium mobilization and chemotaxis induced by CKLF1-C27 through the CCR4 were investigated. HEK293-CCR4 cells 2# were pretreated with **41** (1×10^{-5} M) for 1 h at 37 °C. CKLF1-C27 was administered at 30 s. As indicated in Figure 5, CKLF1-C27 induced calcium mobilization quickly and persistently (parts a1−a4 of Figure 5A). However, compound **41** strongly interrupted the calcium mobilization induced by CKLF1-C27 (parts b1−b4 of Figure 5A). A time curve of CKLF1-C27 stimulation of HEK239-CCR4 2# cells was recorded that did not occur when the cells were incubated with CKLF1-C27 and **41**, or **41** alone (Figure 5B). A chemotaxis assay was then performed. As shown in Figure 6A, maximum chemotaxis was observed at 200 nM CKLF1-C27. Compound **41** efficiently decreased the chemotaxis index (CI) of HEK293-CCR4 2# cells induced by CKLF1-27 in a dose-dependent manner (Figure 6B).

Anti-Inflammatory Activity of Compound 41 in Asthmatic Mice. CKLF1 is thought to play a role in the pathological progress of human asthma.[23] Asthma was recently accepted as a Th2 lymphocyte-mediated chronic inflammatory disorder.[33] In this study, we administrated asthmatic mice[26] with compound **41** to investigate the suppression of the asthmatic inflammation induced by overexpression of CKLF1. CKLF1 was expressed more in pCDI-CKLF1-electroporated mice than in pCDI-transfected mice (Figure 7A). Extensive morphological changes in the lung tissue of human CKLF1-electroporated mice were observed after the mice were electroporated by human pCDI-CKLF1 for 3 weeks. Perivascular and peribronchiolar inflammatory cell infiltration was diagnosed on the basis of the observation of light fusion of the alveolar septae in p-CDI-transfected mice (Figure 7C), however, stronger in human pCDI-CKLF1-electroporated mice (Figure 7B). Mice treated with dexamethasone (DEX, 2 mg, kg^{-1}, Figure 7D) or **41** (120 mg, kg^{-1}, Figure 7F) had significantly less infiltration of inflammatory cells, suggesting that they were

Scheme 4. Synthesis of the Target Compounds **41**−**46**[a]

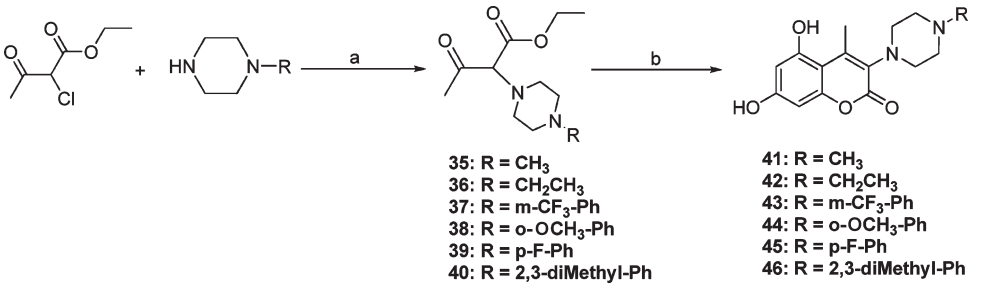

[a] Reagents and conditions: (a) K_2CO_3, ACN, 50 °C; (b) pholoroglucinol, $BF_3 \cdot Et_2O$, EtOH.

Scheme 5. Synthesis of the Compounds **47**[a]

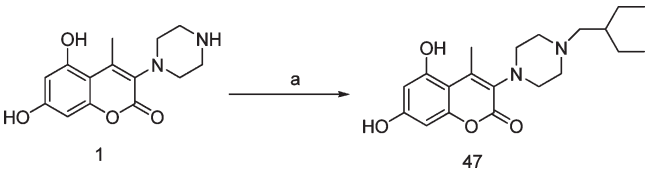

[a] Reagents and conditions: $(CH_3CH_2)_2CHCHO$, $NaBH_3CN$, CH_3OH, room temp.

Scheme 6. Synthesis of Aimed Compounds **49**−**54**[a]

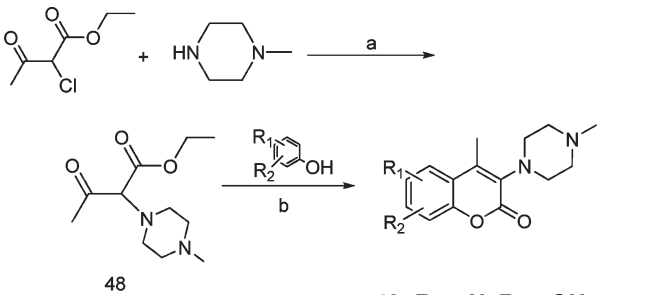

49: R_1 = H, R_2 = OH
50: R_1 = OH, R_2 = CH_3
51: R_1 = R_2= [1,3]dioxole
52: R_1 =OH, R_2 = OCH_3
53: R_1 = R_2 =OCH_3
54: R_1 =$(CH_3)_2N$

[a] Reagents and conditions: (a) K_2CO_3, CH_3CN, 50 °C; (b) $BF_3 \cdot Et_2O$, EtOH.

Scheme 7. Synthesis of the Aimed Compounds **55**−**62**[a]

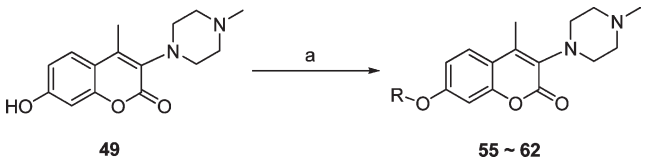

[a] Reagents and conditions: (a) ROH, PPh_3, DEAD, THF, room temp.

protected from developing peribronchial inflammation and fusion of the alveolar septae. In addition, more collagen, indicating lung fibrosis,[26] was also found around the trachea and vascular areas in lung tissue of human CKLF1-electroporated mice (Figure 8B) than in pCDI-transfected mice (Figure 8A). DEX (2 mg, kg^{-1}, Figure 8C) and **41** (20 mg, kg^{-1} and 120 mg, kg^{-1}, Figure 8D, E) obviously attenuated collagen deposition and thus prevented fibrotic progress in the lungs of the mice.

The white blood cell (WBC) and eosinophil (EOS) counts in bronchoalveolar lavage fluid (BALF) were higher in human CKLF1-electroporated mice than in human pCDI-electroporated mice (Table 5). DEX (2 mg, kg^{-1}) administration (ip) to a control group effectively reduced the numbers of WBCs and EOSs in human CKLF1-electroporated mice. Although oral administration of **41** at 20 mg, kg^{-1} for 3 weeks did not have a significant effect, the transfected mice treated with 120 mg, kg^{-1} of **41** had fewer WBCs than those associated with inflammation in human CKLF1-electroporated mice (Table 5). EOSs play a crucial role in the ongoing inflammation through either impaired clearance or delayed apoptosis in the airways.[34] Previous data further support the notion that morphologic changes in airway tissue of mice and the severity of asthma correlate with the presence of activated

Table 4. 5,7-Dihydroxyl Derivated C3-Piperazinecoumarin Analogues and Their Inhibitory Potency

Compd	Structure	IC_{50}	Compd	Structure	IC_{50}
49	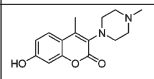	7.75×10^{-7}	56	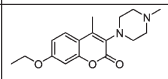	1.64×10^{-6}
50	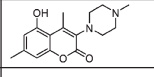	1.13×10^{-6}	57	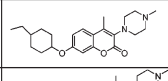	3.12×10^{-6}
51	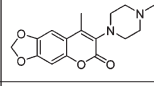	4.20×10^{-7}	58	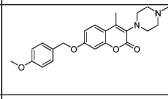	7.32×10^{-6}
52	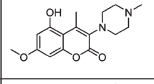	3.89×10^{-7}	59	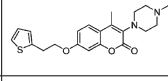	5.27×10^{-7}
53	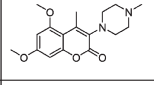	4.78×10^{-7}	60	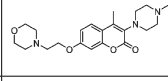	6.71×10^{-7}
54	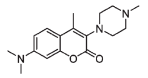	4.76×10^{-6}	61	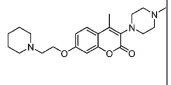	1.96×10^{-7}
55	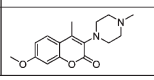	5.21×10^{-6}	62	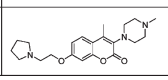	1.51×10^{-6}

airway inflammatory cells, in particular EOSs.[35] As shown in Table 5, both DEX at 2 mg, kg^{-1} and **41** at 120 mg, kg^{-1} significantly decreased the accumulation of EOSs, which reduced the inflammatory lesions in the lung tissue (Figure 7D, F).

Mechanism of Action of Compound 41. In chronic inflammatory diseases such as asthma, several cytokines recruit activated immune and inflammatory cells to the sites of lesions, thereby amplifying and perpetuating the inflammatory state.[36] These activated cells produce many other mediators of inflammation. What causes these diseases is still a mystery, but the interplay of genetic and environmental factors is accepted as playing a role. One ubiquitous transcription factor of particular importance in immune and inflammatory responses is NF-κB.[38] NF-κB increases the expression of the genes for many cytokines, enzymes, and adhesion molecules in chronic inflammatory diseases. Overactivation of NF-κB orchestrates airway eosinophilia and pathologic changes in the lung in asthma patients.[39] Activation of NF-κB involves the phosphorylation and subsequent proteolytic degradation of the inhibitory protein IκB by IκB kinases. Free NF-κB (a heterodimer of p50 and p65) then passes into the nucleus, where it binds to κB sites in the promoter regions of genes for inflammatory proteins such as cytokines, enzymes, and adhesion molecules.[40−42]

Han et al. found that the pathological changes in the lungs of human CKLF1-electroporated mice were similar to those observed in asthma patients.[23] We postulated that the inflammatory lung lesions in CKLF1-electroporated mice are associated with NF-κB signal dysregulation caused by the activation of pulmonary NF-κB by CKLF1. The human CKLF1-electroporated mice showed a significantly up-regulated expression of p-IκB (Figure 9A, lane 2), whereas the pulmonary cytoplasmic IκBα expression in the lung lysate was down-regulated as shown by degraded polyubiquitination (Figure 9B, lane 2). The release of NF-κB from IκB resulted in the passage of NF-κB into the nucleus, and the level of NF-κB (p65) decreased significantly in the cytoplasm (Figure 9C, lane 2). The level of p-IκB decreased significantly in groups treated with **41** or DEX (Figure 9A, lanes 3−5), which increased the IκB level in the cytoplasm (Figure 9B, lanes 3−5), indicating

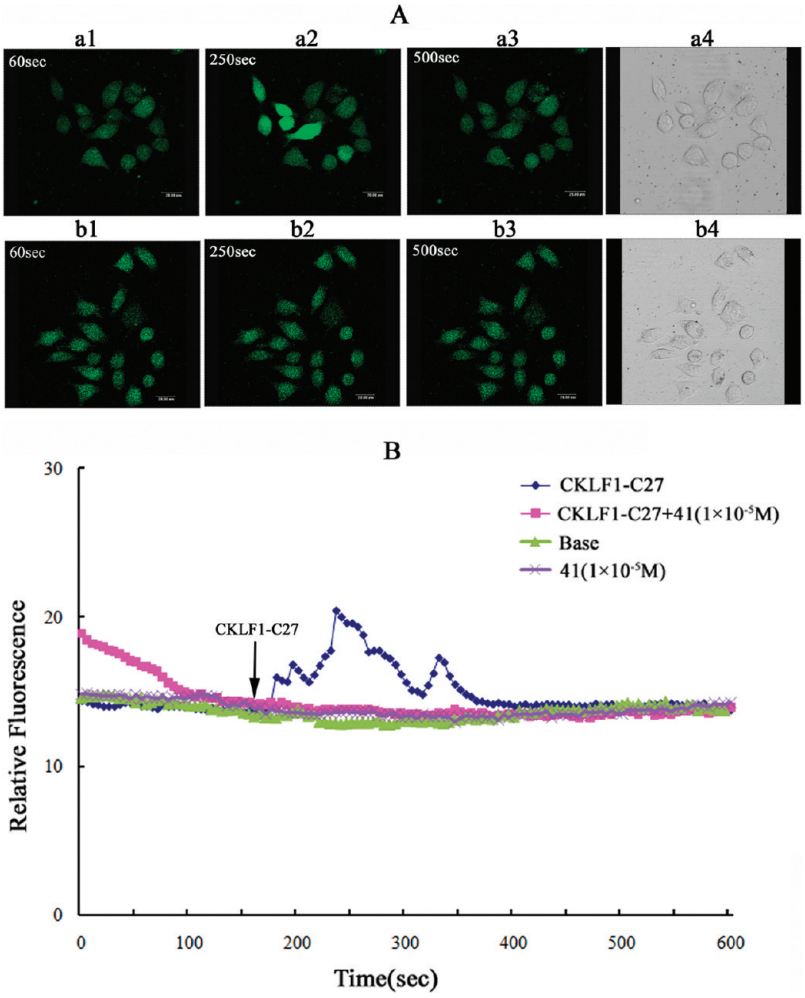

Figure 5. The calcium concentration in HEK293-CCR4 2# cells was measured by confocal microscopic scanning in the absence (a1−a4) or the presence of compound **41** (b1−b4). Parts a4 and b4 were recorded under the visible vision. (A) Parts a1 and b1 were recorded at 60 s in the absence of CKLF1-C27. Parts a2 and b2 were stimulated with CKLF1-C27 at 250 s; parts a3 and b3 were observed at 500 s (bar = 20 μm). (B) The time curve of fluorescence released after CKLF1-C27 stimulation of HEK293-CCR4 2# cells (n = 3).

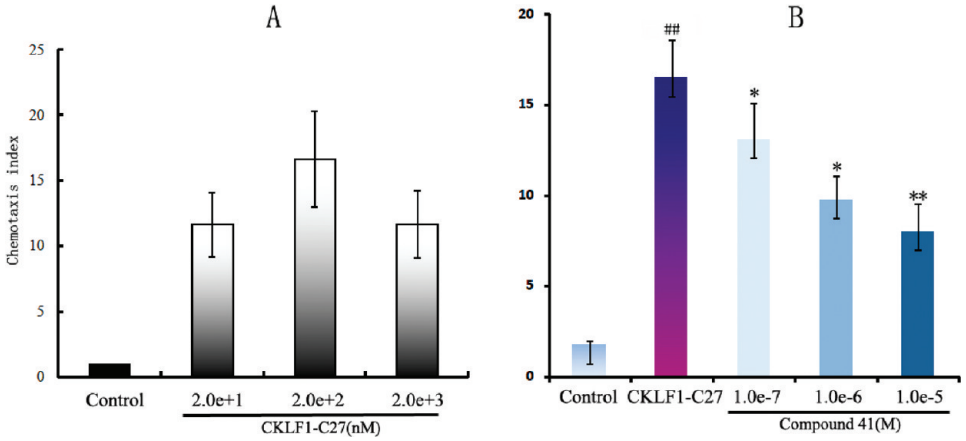

Figure 6. Compound **41** decreased the chemotaxis induced by CKLF1-27. (A) The maximum chemotaxis of HEK293-CCR4 2# cells was at a CKLF1-C27 concentration of 200 nM. (B) **41** dose-dependently inhibited the CI induced by CKLF1-C27 at 200 nM. The controls were untreated HEK293-CCR4 2# cells: (##) $p < 0.001$ vs control group; (*) $p < 0.05$ vs CKLF1-C27 group; (**) $p < 0.01$ vs CKLF1-C27 group.

that the polyubiquitination of IκB was inhibited. Finally, the NF-κB in the cytoplasm was recovered in human CKLF1-transfected mice (Figure 9C, lanes 3−5). We also observed a high negative correlation between EOS recruitment in the BALF and the level of NF-κB in the cytoplasm (γ = −0.83), indicating that the EOS number in the BALF decreased when NF-κB was up-regulated in the cytoplasm.

Taken together, our data support a plausible mechanism by which **41** inhibits the activation of NF-κB by interfering with the binding between CCR4 and CKLF1. The overactivation

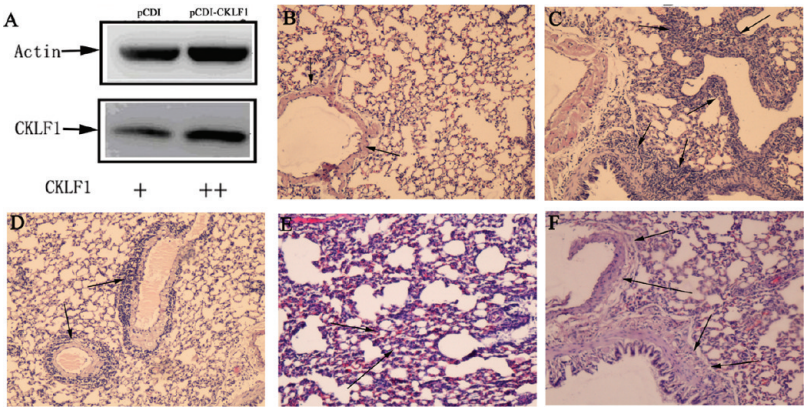

Figure 7. Overexpression of human CKLF1 induced morphological changes (arrows) in the lungs of mice, shown by hematoxylin and eosin (HE) staining: (A) expression of human CKLF1 in lung tissue was analyzed by Western blotting; (B) human pCDI-electroporated mice; (C) human CKLF1-electroporated mice; (D) DEX-treated human CKLF1-electroporated mice; (E) compound **41**-treated human CKLF1-electroporated mice (20 mg, kg^{-1}); (F) compound **41**-treated human CKLF1-electroporated mice (120 mg, kg^{-1}) ($n = 5$, 100×).

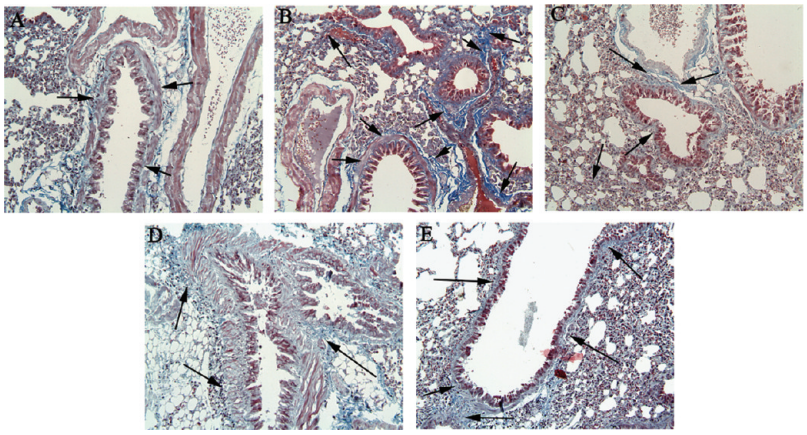

Figure 8. Collagen deposition in lung tissue of mice is indicated by arrows: (A) pCDI-electroporated mice; (B) human CKLF1-electroporated mice; (C) DEX-treated human CKLF1-electroporated mice; (D) compound **41**-treated human CKLF1-electroporated mice (20 mg, kg^{-1}); (E) compound **41**-treated human CKLF1-electroporated mice (120 mg, kg^{-1}) ($n = 5$, 100×).

Table 5. WBC and EOS Counts in BALF (Mean ± SD)[a]

group	dose (mg/kg)	WBC ($10^3/\mu$L)	eosinophils (%)
human pCDI		0.37 ± 0.08	0.82 ± 0.10
human pCDI-CKLF1		0.76 ± 0.16##	1.76 ± 0.21##
DEX	2	0.54 ± 0.09**	0.77 ± 0.11**
41	120	0.38 ± 0.11**	0.79 ± 0.13**
41	20	0.72 ± 0.13	1.13 ± 0.15*

[a] (##) $P < 0.01$ vs control group. (*) $P < 0.05$, (**) $P < 0.01$ vs model group.

of the NF-κB signal pathway was reduced by **41** in human CKLF1-transfected mice.

In summary, we have successfully established a cell-based screening assay of the CKLF1-CCR4 interaction using FITC-labeled CKLF1-C27. Screening of our in-stock small-molecule library and medicinal optimization of an identified coumarin analogue **1** ($IC_{50} = 4.36 \times 10^{-6}$ M) in vitro led to the discovery of potent **41** ($IC_{50} = 2.12 \times 10^{-8}$ M). Compound **41** blocked calcium mobilization and chemotaxis induced by CKLF1-C27. Compound **41** lessened the asthmatic pathologic changes and collagen deposition in the lung tissues and decreased the accumulation of EOSs in the BALF in human CKLF1-transfected mice. Our data demonstrate that the anti-inflammatory activity of **41** in asthmatic mice led to the inhibition of NF-κB activation by reducing the phosphorylation of IκB in the airways and by inhibiting the degradation of IκB in the cytoplasm. As a final result, the abnormal translocation of NF-κB into the nucleus was stopped by **41**, and the pathologic changes in lung tissue were attenuated. These observations indicate that **41** or its analogues have potential as a treatment for patients with asthma.

Experimental Section

Chemistry. All chemical reagents were purchased from Alfa Aesar Co. Ltd. and Acros Organics (Geel, Belgium) and used without further purification. All NMR experiments were carried out on a Varian Mercury 300 or 400 or 500 MHz NMR spectrometer using DMSO-d_6 as the solvent. Chemical shifts were reported in ppm (δ) relative to the solvent signal, and coupling constants (J) were reported in Hz. Melting points are uncorrected and measured with the Yanoco micromelting point apparatus. Automatic HPLC−MS analysis was performed on a ThermoFinnigan LCQ-Advantage mass spectrometer equipped with an Agilent pump, an Agilent detector, an Agilent liquid handler, and a fluent splitter. The employed column was a Kromasil C18 column (4.6 μm, 4.6 mm × 50 mm) from DIKMA for analysis. The eluent was a mixture of acetonitrile and water containing 0.05% HCOOH with a linear gradient from 5:95 (v:v) to 95:5 (v:v) of acetonitrile−H_2O within 5 min at a 1 mL/min flow rate for analysis. The UV detection was carried out at a UV wavelength of 254 nm. Then 5% of the eluent was split into

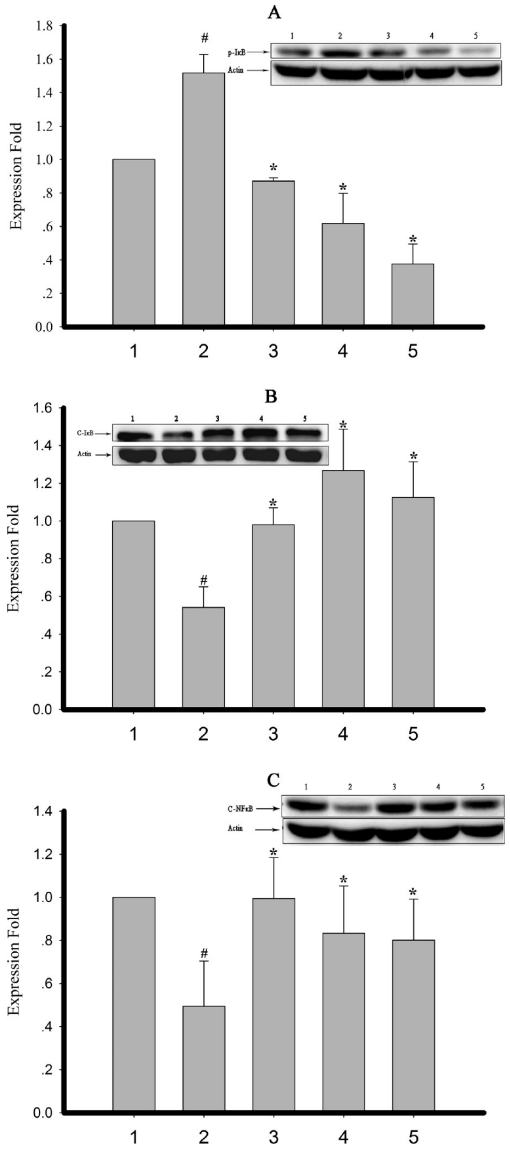

Figure 9. Compound **41** inhibited NF-κB activation in human CKLF1-electroporated mice. (A) The p-IκB level in lung tissue of human CKLF1-electroporated mice was reduced by compound **41**. (B) The IκB in the cytoplasm was degraded in human CKLF1-electroporated mice, although **41** inhibited the degradation. (C) **41** blocked the transfer of NF-κB into the cytoplasm. The data are presented as the mean ± SD (n = 3): (lane 1) mice transfected with human pCDI′; (lane 2) mice electroporated with human pCDI-CKLF1; (lane 3) human CKLF1-electroporated mice treated with DEX (2 mg, kg^{-1}). Lanes 4 and 5 were the human CKLF1-electroporated mice that were treated with 20 and 120 mg, kg^{-1} **41**, respectively.

the MS system. Mass spectra were recorded in either positive or negative ion mode using electrospray ionization (ESI). High resolution LC−MS was carried out by Agilent LC/MSD TOF using a column of Agilent ZORBAX SB-C18 (rapid resolution, 3.5 μm, 2.1 mm × 30 mm) at a flow of 0.40 mL/min. The solvent is methanol/water = 75:25 (v:v) containing 5 mmol/L ammonium formate. The ion source is electrospray ionization (ESI). Flash column chromatography was performed with silica gel 60 (200−300 mesh) from Qindao Haiyang Chemical Factory. All tested compounds were purified until the purity was ≥95%, detected by HPLC under UV 254 nm wavelength, NMR, melting point, and HR LC−MS.

5,7-Dihydroxy-4-methyl-3-morpholino-2*H*-chromen-2-one (21). To a mixture of pholoroglucinol (1.26 g, 10 mmol) and 2-chloro-β-ketoethyl acetate (1.65 g, 10 mmol) was added 50 mL of methanol saturated with dry HCl gas under stirring until completely dissolved at room temperature. The precipitate was then collected by filtration and dried to give **11** as an off-white solid. Then **11** was dissolved in the pyridine (50 mL), and to it was added morpholine (851 mg, 10 mmol). The mixture was refluxed until **11** had completely disappeared as monitored by fast LC−MS analysis. The solution was concentrated in vacuo. The final product **21** was obtained in 12.3% yield as a light-brown solid and characterized after chromatographic purification on silica gel. Mp 224−226 °C. ^{1}H NMR (300 MHz, DMSO-d_6): δ 6.375 (d, 1H, J = 2.1 Hz), 6.116 (d, 1H, J = 2.1 Hz), 3.354 (br, 4H), 2.601 (s, 3H), 1.546 (br, 6H). HRMS calcd for $C_{15}H_{18}NO_4$ ($M + H^+$) 276.1236; found 276.1239.

5,7-Dihydroxy-4-methyl-3-(piperidin-1-yl)-chromen-2-one (22). The title compound was prepared in a manner similar to **21** with the replacement of morpholine with piperidine to afford after chromatography the celadon solid (423 mg, 15.3%). Mp 285−287 °C. ^{1}H NMR (300 MHz, DMSO-d_6): δ 10.404 (s, 1H), 10.175 (s, 1H), 6.249 (d, 1H, J = 2.1 Hz), 6.117 (d, 1H, J = 2.1 Hz), 3.641 (br, 4H), 2.858 (br, 4H). 2.644 (s, 3H). HRMS calcd for $C_{14}H_{16}NO_5$ ($M + H^+$) 278.1028; found 278.1028.

5,7-Dihydroxy-4-methyl-3-phenyl-2*H*-chromen-2-one (23). This procedure was performed according to a modified literature procedure.[44] A mixture of 2,4,6-trihydroxyacetophenone (168 mg, 1 mmol) and phenylacetyl chloride (440 μL, 3 mmol) in acetone in the presence of insoluble materials (510 mg, 3 mmol) was refluxed until the material completely disappeared. Insoluble materials were filtered, and solvent was removed. The residue was purified to yield compound **23** as a white powder (203 mg, 76.0%). Mp 263−265 °C. ^{1}H NMR (300 MHz, DMSO-d_6): δ 10.405 (br, 2H), 7.310−7.430 (m, 3H), 7.204−7.227 (m, 2H), 6.295 (d, 1H, J = 2.1 Hz), 6.192 (d, 1H, J = 2.1 Hz), 2.318 (s, 3H). ^{13}C NMR (125 MHz, DMSO-d_6): δ 160.693, 160.025, 158.225, 155.337, 150.081, 135.564, 130.453, 128.069, 127.271, 120.783, 102.356, 99.423, 94.255, 20.939. HRMS calcd for $C_{16}H_{13}O_4$ ($M + H^+$) 269.0814; found 269.0782.

5,7-Dihydroxy-4-methyl-3-(piperazin-1-yl)-2*H*-chromen-2-one (1). To a mixture of anhydrous piperazine (4.30 g, 50 mmol) and anhydrous K_2CO_3(7.60 g, 55 mmol) in acetonitrile (150 mL) was added dropwise 2- chloro-β-ketoethyl acetate (8.23 g, 6.92 mL) at room temperature. The mixture was stirred for 1 h. The solvent was evaporated in vacuo, and water was added to the residue. The resulting mixture was extracted with EtOAc (3 × 100 mL). The organic layers were combined, dried completely over anhydrous Na_2SO_4, and evaporated in vacuo to give a brown oil. To a solution of the resulting oil and pholoroglucinol (6.3 g, 50 mmol) in absolute ethanol (100 mL) was added 40 mL of $BF_3 \cdot Et_2O$ at room temperature. The mixture was refluxed until the reaction was completed as monitored by fast LC−MS analysis. The resulting solid was eluted by Et_2O to give **1** as an off-white powder (9.38 g, 68.0% yield). Mp 110−112 °C. ^{1}H NMR (300 MHz, DMSO-d_6): δ 6.233 (d, 1H, J = 2.1 Hz), 6.092 (d, 1H, J = 2.1 Hz), 3.156 (br, 4H), 2.799 (br, 5H), 2.624 (s, 3H). HRMS calcd for $C_{14}H_{17}N_2O_4$ ($M + H^+$) 277.1188; found 277.1183.

General Procedure a for Synthesis of Compounds 24−27. To a solution of **1** (27.6 mg, 0.1 mmol) in 5 mL of dry THF aided by DMF, Et_3N (30 mg, 0.3 mmol) and acyl chloride (0.3 mmol) were added. The reaction mixture was stirred at 45 °C. After the reaction was completed, the solvent was evaporated in vacuo. The final products were characterized after purification by silica gel column chromatography.

3-(4-Cinnamoylpiperazin-1-yl)-5,7-dihydroxy-4-methyl-2*H*-chromen-2-one (24). White solid in 46% yield. Mp 232−234 °C. ^{1}H NMR (300 MHz, DMSO-d_6): δ 10.433 (s, 1H), 10.196 (s, 1H), 7.722 (d, 2H, J = 7.5 Hz, J = 1.5 Hz), 7.515 (d, 1H, J = 15.6 Hz), 7.356−7.430 (m, 3H), 7.300 (d, 1H, J = 15.6 Hz), 6.260 (d, 1H, J = 2.4 Hz), 6.120 (d, 1H, J = 2.4 Hz), 3.315−4.448 (br, 4H), 2.710−3.165 (br, 4H), 2.681 (s, 3H). ^{13}C NMR (125 MHz, DMSO-d_6): δ 164.406, 160.202, 157.978,

157.888, 154.525, 150.054, 141.505, 135.158, 129.474, 128.715, 128.015, 118.268, 102.219, 99.318, 94.102, 49.817, 49.087, 45.895, 42.451, 17.004. HRMS calcd for $C_{23}H_{23}N_2O_5$ ($M + H^+$) 407.1607; found 407.1594.

3-(4-Acryloylpiperazin-1-yl)-5,7-dihydroxy-4-methyl-2*H*-chromen-2-one (25). Off-white solid in 62.7% yield. Mp 225−228 °C. ^{1}H NMR (300 MHz, DMSO-d_6): ^{1}H NMR (300 MHz, DMSO-d_6): δ 10.422 (s, 1H), 10.186 (s, 1H), 6.825 (dd, 1H, J = 12.6 Hz, J = 7.8 Hz), 6.256 (d, 1H, J = 1.2 Hz), 6.121 (dd, 1H, J = 12.6 Hz, J = 1.5 Hz), 6.118 (d, 1H, J = 1.2 Hz), 5.680 (d, 1H, J = 7.8 Hz, J = 1.2 Hz), 2.720−4.501 (br, 8H), 2.660 (s, 3H). HRMS calcd for $C_{17}H_{19}N_2O_5$ ($M + H^+$) 331.1294; found 331.1280.

3-(4-(2-Chloroacetyl)piperazin-1-yl)-5,7-dihydroxy-4-methyl-2*H*-chromen-2-one (26). White solid in 58.4% yield. Mp 262−264 °C. ^{1}H NMR (300 MHz, DMSO-d_6): δ 10.428 (s, 1H), 10.193 (s, 1H), 6.260 (d, 1H, J = 2.4 Hz), 6.120 (d, 1H, J = 2.4 Hz), 4.401 (s, 2H), 2.654−4.401 (br, 8H), 2.654 (s, 3H). HRMS calcd for $C_{16}H_{18}ClN_2O_5$ ($M + H^+$) 353.0904; found 353.0900.

3-(4-benzoylpiperazin-1-yl)-5,7-dihydroxy-4-methyl-2H-chromen-2-one (27). White solid in 50.2% yield. Mp 260−262 °C. ^{1}H NMR (300 MHz, DMSO-d_6): δ 10.421 (s, 1H), 10.187 (s, 1H), 7.396−7.458 (m, 5H), 6.254 (d, 1H, J = 1.8 Hz), 6.125 (d, 1H, J = 1.8 Hz), 2.658−4.500 (br, 8H), 2.658 (s, 3H). HRMS calcd for $C_{21}H_{21}N_2O_5$ ($M + H^+$) 381.1450; found 381.1449.

General Procedure B for Synthesis of Compounds 28 and 29. To a solution of **1** (27.6 mg, 0.1 mmol) in 5 mL of dried DCM were added pyridine (23.7 mg, 0.3 mmol) and sulfonyl chloride (0.3 mmol). The reaction mixture was stirred at 45 °C. Chemical conversion was monitored by LC−MS analysis. After the reaction was completed, the solvent was evaporated in vacuo. Water was added and then extracted twice using ethyl acetate (30 mL × 2). The combined organic layers were washed with brine, dried over anhydrous sodium sulfate, and concentrated in vacuo to give crude products. The final **28** and **29** were characterized after purification by silica gel column chromatography.

5,7-Dihydroxy-4-methyl-3-(4-(phenylsulfonyl)piperazin-1-yl)-2*H*-chromen-2-one (28). White solid in 13.6% yield. Mp 231−234 °C. ^{1}H NMR (300 MHz, DMSO-d_6, 80 °C): δ 10.400 (s, 1H), 10.201 (s, 1H), 7.710 (m, 5H), 6.226 (d, 1H, J = 2.4 Hz), 6.105 (d, 1H, J = 2.4 Hz), 3.855 (br, 1H), 3.187 (br, 3H), 2.997 (br, 4H), 2.487 (s, 3H). HRMS calcd for $C_{20}H_{20}N_2NaO_6S$ ($M + Na^+$) 439.0940; found. 439.0932.

***N*-(4-(4-(5,7-Dihydroxy-4-methyl-2-oxo-2*H*-chromen-3-yl)-piperazin-1-ylsulfonyl)phenyl)acetamide (29).** White solid in 20.5% yield. Mp 258−260 °C. ^{1}H NMR (300 MHz, DMSO-d_6): 10.399 (s, 1H), 10.194 (s, 1H), 7.941 (s, 1H), 7.817 (m, 2H), 7.489 (m, 2H), 6.230 (d, 1H, J = 2.4 Hz), 6.108 (d, 1H, J = 2.4 Hz), 2.522−3.551 (br, 8H), 2.878 (s, 3H), 2.720 (s, 3H). HRMS calcd for $C_{22}H_{24}N_3O_7S$ ($M + H^+$) 474.1335; found. 474.1308.

General Procedure C for Synthesis of Compounds 30−34. To a solution of **1** (55.2 mg, 0.2 mmol) in 5 mL of dry THF and a little DMF, various isocyanates (0.24 mmol) were added, and the reaction mixture was stirred at 50 °C. After the reaction was completed, the solvent was evaporated in vacuo. The final products were characterized after purification by silica gel column chromatography.

4-(5,7-Dihydroxy-4-methyl-2-oxo-2*H*-chromen-3-yl)-*N*-(4-isopropylphenyl)piperazine-1-carboxamide (30). Off-white solid in 25.3% yield. Mp 262−265 °C. ^{1}H NMR (300 MHz, DMSO-d_6): δ 10.421 (s, 1H), 10.186 (s, 1H), 8.441 (s, 1H), 7.348 (dd, 2H, J = 8.7 Hz, J = 1.5 Hz), 7.082 (dd, 2H, J = 8.7 Hz, J = 1.5 Hz), 6.258 (d, 1H, J = 2.4 Hz), 6.124 (d, 1H, J = 2.4 Hz), 3.459 (s, 1H), 2.779−4.400 (br, 8H), 2.668 (s, 3H), 1.174 (s, 3H), 1.151 (s, 3H). HRMS calcd for $C_{24}H_{28}N_3O_5$ ($M + H^+$) 438.2029; found 438.2007.

4-(5,7-Dihydroxy-4-methyl-2-oxo-2*H*-chromen-3-yl)-*N*-heptylpiperazine-1-carboxamide (31). Off-white powder in 56.0% yield. Mp 282−284 °C. ^{1}H NMR (400 MHz, DMSO-d_6): δ 10.400 (s, 1H), 10.170 (s, 1H), 6.450 (t, 1H, J = 5.1 Hz), 6.249 (d, 1H, J = 2.1 Hz), 6.110 (d, 1H, J = 2.1 Hz), 3.000 (m, 2H, J = 6.0 Hz), 2.638−4.000 (br, 8H), 2.638 (s, 3H), 1.162−1.412 (m, 10H, J = 6.0 Hz), 0.845 (t, 3H, J = 6.0 Hz). HRMS calcd for $C_{22}H_{32}N_3O_5$ ($M + H^+$) 418.2342; found 418.2342.

4-(5,7-Dihydroxy-4-methyl-2-oxo-2*H*-chromen-3-yl)-*N*-(2-phenoxyphenyl)piperazine-1-carboxamide (32). White powder in 32.6% yield. Mp 198−200 °C. ^{1}H NMR (300 MHz, DMSO-d_6): δ 10.424 (s, 1H), 10.194 (s, 1H), 7.975 (s, 1H), 7.665 (d, 1H, J = 7.5 Hz), 7.340 (t, 2H, J = 7.5 Hz), 7.079 (m, 3H), 6.930 (m, 3H), 6.251 (s, 1H), 6.117 (s, 1H), 2.000−4.000 (br, 8H), 2.623 (s, 3H). HRMS calcd for $C_{27}H_{26}N_3O_6$ ($M + H^+$) 488.1822; found 488.1810.

4-(5,7-Dihydroxy-4-methyl-2-oxo-2*H*-chromen-3-yl)-*N*-(4-(trifluoromethoxy)phenyl)piperazine-1-carboxamide (33). White powder in 41.2% yield. Mp 254−256 °C. ^{1}H NMR (300 MHz, DMSO-d_6, 80 °C): δ 10.202 (s, 1H), 9.952 (s, 1H), 8.741 (s, 1H), 7.570 (d, 2H, J = 4.5 Hz), 7.200 (d, 2H, J = 4.5 Hz), 6.272 (d, 1H, J = 1.2 Hz), 6.132 (d, 1H, J = 1.2 Hz), 3.524 (br, 4H), 2.961 (br, 4H), 2.685 (s, 3H). ^{13}C NMR (125 MHz, DMSO-d_6): δ 160.082, 157.855, 154.677, 154.452, 149.791, 142.460, 139.836, 128.153, 120.467, 120.012, 102.204, 99.204, 94.041, 48.994, 44.455, 16.858. HRMS calcd for $C_{22}H_{21}F_3N_3O_6$ ($M + H^+$) 480.1382; found 480.1387.

***N*-Benzyl-4-(5,7-dihydroxy-4-methyl-2-oxo-2*H*-chromen-3-yl)piperazine-1-carboxamide (34).** Yellow powder in 41.8% yield. Mp 277−280 °C. ^{1}H NMR (300 MHz, DMSO-d_6): δ 10.409 (s, 1H), 10.177 (s, 1H), 7.168−7.355(m, 5H), 7.096 (t, 1H, J = 6.0 Hz), 6.250 (d, 1H, J = 2.4 Hz), 6.120 (d, 1H, J = 2.4 Hz), 4.250 (d, 2H, J = 6.0 Hz), 3.322−4.100 (m, 4H), 2.925 (br, 4H), 2.878 (s, 3H). ^{13}C NMR (125 MHz, DMSO-d_6): δ 160.098, 157.900, 157.450, 154.502, 149.780, 141.007, 128.339, 128.046, 126.940, 126.345, 102.299, 99.351, 94.094, 59.708, 49.001, 44.264, 16.889. HRMS calcd for $C_{22}H_{24}N_3O_5$ ($M + H^+$) 410.1716; found 410.1711.

General Procedure D for Synthesis of Compounds 41−46. To a mixture of various substitutional piperazines (1 mmol) and anhydrous K_2CO_3 (165.8 mg,1.2 mmol) in acetonitrile (20 mL) was added dropwise 2-chloro-β-ketoethyl acetate (164.6 mg, 1 mmol) at room temperature. The mixture was stirred for 3 h. The solvent was evaporated in vacuo, and water was added. The resulting mixture was extracted with EtOAc (3 × 30 mL). The organic layers were combined, dried completely over anhydrous Na_2SO_4, and evaporated in vacuo to give a yellow oil (**35**−**40**). Then the resulting oil and pholoroglucinol (126.1 mg, 1 mmol) were dissolved in absolute ethanol (10 mL). $BF_3 \cdot Et_2O$ (617 μL, 5 mmol) was added at room temperature, and the mixture was refluxed until the reaction was completed as monitored by fast LC−MS analysis. The solvent was evaporated in vacuo and the resulting residue was eluted using dichloromethane to give the final products.

5,7-Dihydroxy-4-methyl-3-(4-methylpiperazin-1-yl)-2*H*-chromen-2-one (41). Off-white powder in 87.5% yield. Mp 208−210 °C. ^{1}H NMR (500 MHz, DMSO-d_6, 75 °C): δ 6.259 (d, 1H, J = 2.5 Hz), 6.114 (d, 1H, J = 2.5 Hz), 2.935−2.955 (br, 4H), 2.624 (s, 3H), 2.400−2.482 (br, 4H), 2.235 (s, 3H). HRMS calcd for $C_{15}H_{19}N_2O_4$ ($M + H^+$) 291.1345; found 291.1344.

3-(4-Ethylpiperazin-1-yl)-5,7-dihydroxy-4-methyl-2*H*-chromen-2-one (42). Light-yellow powder in 85.4% yield. Mp 210−212 °C. ^{1}H NMR (300 MHz, DMSO-d_6): δ 10.535 (s, 1H), 10.288 (s, 1H), 9.542 (s, 1H), 6.317 (d, 1H, J = 2.4 Hz), 6.135 (d, 1H, J = 2.4 Hz), 3.428−3.539 (br, 4H), 3.058−3.149 (br, 4H), 2.850 (br, 2H), 2.637 (s, 3H), 1.229 (t, 3H, J = 7.5 Hz). HRMS calcd for $C_{16}H_{21}N_2O_4$ ($M + H^+$) 305.1501; found 305.1505.

5,7-Dihydroxy-4-methyl-3-(4-(3-(trifluoromethyl)phenyl)piperazin-1-yl)-2*H*-chromen-2-one (43). Yellow powder in 52.5% yield. Mp 235−238 °C. ^{1}H NMR (300 MHz, DMSO-d_6): δ 10.426 (s, 1H), 10.190 (s, 1H), 7.418, t, 1H, J = 7.8 Hz), 7.245 (d, 1H, J = 7.8 Hz), 7.188 (s, 1H), 7.065 (d, 1H, J = 7.8 Hz), 6.260 (d, 1H, J = 2.4 Hz), 6.128 (d, 1H, J = 2.4 Hz), 2.879−4.231 (br,

8H), 2.666 (s, 3H). HRMS calcd for $C_{21}H_{20}F_3N_2O_4$ ($M + H^+$) 421.1375; found 421.1378.

5,7-Dihydroxy-3-(4-(2-methoxyphenyl)piperazin-1-yl)-4-methyl-2*H*-chromen-2-one (44). Off-white powder in 50.8% yield. Mp 218−221 °C. ^{1}H NMR (300 MHz, DMSO-d_6): δ 10.409 (s, 1H), 10.176 (s, 1H), 7.102 (t, 1H, J = 8.1 Hz), 6.538 (d, 1H, J = 8.1 Hz), 6.468 (m, 1H), 6.358 (d, 1H, J = 8.1 Hz, J = 2.1 Hz), 6.261 (d, 1H, J = 2.4 Hz), 6.130 (d, 1H, J = 2.1 Hz), 3.708 (s, 3H), 2.768−3.465 (br, 8H), 2.660 (s, 3H). HRMS calcd for $C_{21}H_{23}N_2O_5$ ($M + H^+$) 383.1607; found 383.1600.

3-(4-(4-Fluorophenyl)piperazin-1-yl)-5,7-dihydroxy-4-methyl-2*H*-chromen-2-one (45). Off-white powder in 58.0% yield. Mp 189−193 °C. ^{1}H NMR (300 MHz, DMSO-d_6): δ 10.416 (s, 1H), 10.202 (s, 1H), 7.012 (m, 4H), 6.256 (d, 1H, J = 1.5 Hz), 6.130 (d, 1H, J = 1.5 Hz), 2.870−3.438 (br, 8H), 2.653 (s, 3H). HRMS calcd for $C_{20}H_{20}FN_2O_4$ ($M + H^+$) 371.1407; found 371.1405.

3-(4-(2,3-Dimethylphenyl)piperazin-1-yl)-5,7-dihydroxy-4-methyl-2*H*-chromen-2-one (46). Yellow powder in 49.0% yield. Mp 236−239 °C. ^{1}H NMR (300 MHz, DMSO-d_6): δ 10.409 (s, 1H), 10.178 (s, 1H), 7.033 (t, 1H, J = 7.5 Hz, J = 8.1 Hz), 6.931 (t, 1H, J = 8.1 Hz), 6.872 (t, 1H, J = 7.5 Hz), 6.264 (d, 1H, J = 2.4 Hz), 6.139 (d, 1H, J = 2.4 Hz), 3.373 (br, 4H), 2.851 (br, 4H), 2.671 (s, 3H), 2.199 (s, 3H), 2.178 (s, 3H). HRMS calcd for $C_{22}H_{25}N_2O_4$ ($M + H^+$) 381.1814; found 381.1812.

3-(4-(2-Ethylbutyl)piperazin-1-yl)-5,7-dihydroxy-4-methyl-2*H*-chromen-2-one (47). To a solution of **1** (276 mg, 1 mmol) in 30 mL of MeOH was added 2-ethylbutanal (123 μL, 1 mmol), glacial acetic acid (30 μL), and $NaBH_3CN$ (62.8 mg, 1 mmol). The reaction mixture was stirred at 50 °C. Chemical conversion was monitored by LC−MS analysis. After the reaction was complete, the solution was evaporated in vacuo to dryness. The crude residue was dissolved in 30 mL of AcOEt and then washed with saturated $NaHCO_3$ aqueous solution (2 × 10 mL) and brine (2 × 10 mL). After the AcOEt layer was completely dried over anhydrous Na_2SO_4, the filtrate was concentrated in vacuo to obtain the crude product. The final product **47** was purified by silica gel column chromatography using dichloromethane/methanol as the eluent. Yield: 28.5%. Mp 296−299 °C. ^{1}H NMR (300 MHz, DMSO-d_6): δ 5.927 (s, 1H), 5.710 (s, 1H), 2.650−3.685 (br, 8H), 2.650 (s, 3H), 2.120 (d, 2H, J = 4.6 Hz), 1.428 (m, 1H), 1.281 (m, 4H), 0.853 (t, 6H, J = 7.2 Hz). HRMS calcd for $C_{20}H_{29}N_2O_4$ ($M + H^+$) 361.2127; found 361.2124.

7-Hydroxy-4-methyl-3-(4-methylpiperazin-1-yl)-2*H*-chromen-2-one (49). The title compound was prepared in the same manner as compound **41** with replacement of pholoroglucinol with resorcinol to afford **49** as a light-yellow powder in 75.3% yield. Mp 190−192 °C. ^{1}H NMR (300 MHz, DMSO-d_6): δ 7.642 (d, 1H, J = 9.0 Hz), 6.933−6.940 (m, 2H), 3.827 (s, 3H), 2.975 (br, 4H), 2.490 (br, 4H), 2.431 (s, 3H). 2.246 (s, 3H). HRMS calcd for $C_{16}H_{21}N_2O_3$ ($M + H^+$) 289.1552; found 289.1519.

5-Hydroxy-4,7-dimethyl-3-(4-methylpiperazin-1-yl)-2*H*-chromen-2-one Hydrochloride (50). The title compound was prepared in the same manner as compound **41** with replacement of pholoroglucinol with 5-methylbenzene-1,3-diol to afford **50** as a light-yellow powder in 70.5% yield. Mp 213−215 °C. ^{1}H NMR (300 MHz, DMSO-d_6): δ 10.490 (s, 1H), 9.382 (s, 1H), 6.599 (s, 1H), 6.584 (s, 1H), 3.492−3.531 (m, 2H), 3.402−3.445 (m, 2H), 3.105−3.207 (m, 2H), 2.905 (br, 2H), 2.838 (d, 3H, J = 4.2 Hz), 2.674 (s, 3H), 2.262 (s, 3H). ^{13}C NMR (125 MHz, DMSO-d_6): δ 17.118, 20.936, 45.427, 48.452, 54.971, 106.968, 107.296, 111.968, 130.876, 141.373, 148.475, 152.816, 156.382, 157.645. HRMS calcd for $C_{16}H_{21}N_2O_3$ ($M + H^+$) 289.1552; found 289.1553.

8-Methyl-7-(4-methylpiperazin-1-yl)-6*H*-[1,3]dioxolo[4,5-*g*]-chromen-6-one Hydrochloride (51). The title compound was prepared in the same manner as compound **41** with replacement of pholoroglucinol with benzo[*d*][1,3]dioxol-5-ol to afford **51** as a light-yellow powder in 74.5% yield. Mp 254−256 °C. ^{1}H NMR (300 MHz, DMSO-d_6): δ 9.369 (s, 1H), 7.294 (s, 2H), 7.077 (s, 2H), 6.154 (s, 2H), 3.447 (br, 4H), 3.173 (br, 2H), 2.944 (br, 2H), 2.843 (s, 3H), 2.445 (s, 3H). ^{13}C NMR (125 MHz, DMSO-d_6): δ 13.746, 42.536, 46.572, 53.369, 97.474, 102.478, 103.584, 113.788, 129.713, 144.764, 148.056, 148.666, 150.047, 158.171. HRMS calcd for $C_{16}H_{21}N_2O_4$ ($M + H^+$) 305.1501; found 305.1508. HRMS calcd for $C_{16}H_{19}N_2O_4$ ($M + H^+$) 303.1345; found 303.1351.

5-Hydroxy-7-methoxy-4-methyl-3-(4-methylpiperazin-1-yl)-2*H*-chromen-2-one Hydrochloride (52). The title compound was prepared in the same manner as compound **41** with replacement of pholoroglucinol with 5-methoxybenzene-1,3-diol to afford **52** as an off-white powder in 77.0% yield. Mp 173−175 °C. ^{1}H NMR (300 MHz, DMSO-d_6): δ 10.510 (s, 1H), 9.362 (s, 1H), 6.370 (d, 1H, J = 2.1 Hz), 6.280 (d, 1H, J = 2.1 Hz), 3.821 (s, 3H), 3.436−3.483 (br, 4H), 3.132−3.197 (br, 2H), 2.830 (s, 3H), 2.606 (s, 3H).

5,7-Dimethoxy-4-methyl-3-(4-methylpiperazin-1-yl)-2*H*-chromen-2-one Hydrochloride (53). The title compound was prepared in the same manner as compound **41** with replacement of pholoroglucinol with 3,5-dimethoxyphenol to afford **53** as a white powder in 81.0% yield. Mp 230−232 °C. ^{1}H NMR (300 MHz, DMSO-d_6): δ 9.380 (s, 1H), 6.549 (d, 1H, J = 2.4 Hz), 6.510 (d, 1H, J = 2.4 Hz), 3.859 (s, 3H), 3.830 (s, 3H), 3.397−3.485 (m, 4H), 3.178 (br, 2H), 2.892 (br, 2H), 2.839 (s, 3H), 2.620 (s, 3H). ^{13}C NMR (125 MHz, DMSO-d_6): δ 17.214, 42.582, 46.538, 53.379, 55.847, 56.276, 93.228, 95.873, 104.148, 128.642, 154.295, 157.690, 159.161, 162.160. HRMS calcd for $C_{16}H_{21}N_2O_4$ ($M + H^+$) 305.1501; found 305.1508.

7-(Dimethylamino)-4-methyl-3-(4-methylpiperazin-1-yl)-2*H*-chromen-2-one Hydrochloride (54). The title compound was prepared in the same manner as compound **41** with replacement of pholoroglucinol with 3-aminophenol to afford **54** as a light-yellow powder in the 65.0% yield. Mp 163−165 °C. ^{1}H NMR (300 MHz, DMSO-d_6): δ 7.493 (d, 1H, J = 9.0 Hz), 6.722 (d, 1H, J = 9.0 Hz, J = 2.1 Hz), 6.503 (d, 1H, J = 2.1 Hz), 2.600−3.332 (m, 6H), 2.982 (s, 6H), 2.440 (br, 2H), 2.388 (s, 3H), 2.223 (s, 3H). HRMS calcd for $C_{17}H_{24}N_3O_2$ ($M + H^+$) 302.1869; found 302.1872.

General Procedure E for Synthesis of Compounds 55−62. To a mixture of compound **48** (54.8 mg, 0.2 mmol), a commercially available alcohol (0.26 mmol), and PPh_3 (60.9 mg, 0.2 mmol) in anhydrous THF (10 mL) was added DEAD (31.5 μL, 0.2 mmol) at 0 °C. The mixture was allowed to rise to room temperature after addition. Chemical conversion was monitored by LC−MS analysis. After the reaction was completed, the solution was evaporated in vacuo to dryness to obtain the crude product. The final product was purified by silica gel column chromatography using dichloromethane/methanol as the eluent.

7-Methoxy-4-methyl-3-(4-methylpiperazin-1-yl)-2*H*-chromen-2-one (55). Light-yellow powder in 75.3% yield. Mp 190−192 °C. ^{1}H NMR (300 MHz, DMSO-d_6): δ 7.642 (d, 1H, J = 9.0 Hz), 6.933−6.940 (m, 2H), 3.827 (s, 3H), 2.975 (br, 4H), 2.490 (br, 4H), 2.431 (s, 3H). 2.246 (s, 3H). HRMS calcd for $C_{16}H_{21}N_2O_3$ ($M + H^+$) 289.1552; found 289.1519.

7-Ethoxy-4-methyl-3-(4-methylpiperazin-1-yl)-2*H*-chromen-2-one (56). Light-yellow powder in 77.2% yield. Mp 195−197 °C. ^{1}H NMR (300 MHz, DMSO-d_6): δ 7.627 (d, 1H, J = 9.0 Hz), 6.906−6.031 (m, 2H), 4.098 (q, 2H, J = 6.9 Hz), 2.983 (br, 4H), 2.490 (br, 4H), 2.426 (s, 3H), 2.275 (s, 3H), 1.333 (t, 3H, J = 6.9 Hz). HRMS calcd for $C_{17}H_{23}N_2O_{33}$ ($M + H^+$) 303.1709; found 303.1721.

7-(4-Ethylcyclohexyloxy)-4-methyl-3-(4-methylpiperazin-1-yl)-2*H*-chromen-2-one (57). Yellow powder in 54.5% yield. Mp 136−138 °C. ^{1}H NMR (300 MHz, MeOH): δ 7.558 (d, 1H, J = 9.0 Hz), 6.837 (dd, 1H, J = 9.0 Hz, J = 2.4 Hz), 6.749 (d, 1H, J = 2.4 Hz), 4.250 (m, 1H), 3.069 (br, 4H), 2.562 (br, 4H), 2.448 (s, 3H), 2.296 (s, 3H), 2.092 (m, 2H). 1.811 (m, 2H), 0.983−1.425 (m, 8H), 0.863 (t, 3H, J = 7.2 Hz). HRMS calcd for $C_{23}H_{33}N_2O_3$ ($M + H^+$) 385.2491; found 385.2498.

7-(4-Methoxybenzyloxy)-4-methyl-3-(4-methylpiperazin-1-yl)-2*H*-chromen-2-one (58). Light-yellow powder in 68.5% yield.

Mp 182−184 °C. ^{1}H NMR (300 MHz, DMSO-d_6): δ 7.630 (d, 1H, J = 9.0 Hz), 7.385 (d, 2H, J = 9.0 Hz), 6.972−7.003 (m, 2H), 6.937 (d, 2H, J = 9.0 Hz), 5.108 (s, 2H), 3.743 (s, 3H), 2.963 (br, 4H), 2.490 (br, 4H), 2.423 (s, 3H), 2.230 (s, 3H). ^{13}C NMR (125 MHz, DMSO-d_6): δ 12.885, 42.817, 55.099, 59.008, 101.687, 112.042, 112.981, 114.180, 118.799, 127.074, 128.159, 134.255, 148.568, 152.867, 158.084, 160.311, 160.589. HRMS calcd for $C_{23}H_{27}N_2O_4$ ($M + H^+$) 395.1971; found 395.1975.

4-Methyl-3-(4-methylpiperazin-1-yl)-7-(2-(thiophen-2-yl)ethoxy)-2*H*-chromen-2-one (59). Off-white powder in 75.5% yield. Mp 268−270 °C. ^{1}H NMR (300 MHz, DMSO-d_6): δ 7.681 (d, 1H, J = 9.0 Hz), 7.460 (d, 1H, J = 4.5 Hz), 6.962−6.977 (m, 4H), 4.289 (t, 2H, J = 6.0 Hz), 3.271 (t, 2H, J = 6.0 Hz), 3.084 (br, 8H), 2.682 (s, 3H), 2.457 (s, 3H). ^{13}C NMR (125 MHz, DMSO-d_6): δ 13.181, 21.653, 42.910, 101.949, 112.212, 113.181, 125.181, 126.459, 127.290, 127.466, 128.332, 137.826, 149.086, 153.049, 158.339, 160.517. HRMS calcd for $C_{21}H_{25}N_2O_3S$ ($M + H^+$) 385.1586; found 385.1581.

4-Methyl-3-(4-methylpiperazin-1-yl)-7-(2-morpholinoethoxy)-2*H*-chromen-2-one (60). Light-yellow powder in 75.0% yield. Mp 96−98 °C. ^{1}H NMR (300 MHz, DMSO-d_6): δ 7.635 (d, 1H, J = 9.0 Hz), 6.930−6.958 (m, 2H), 3.729 (t, 2H, J = 6.9 Hz), 4.168 (t, 2H, J = 6.0 Hz), 3.533−3.577 (m, 4H), 3.008 (br, 4H), 2.692 (t, 2H, J = 6.0 Hz), 2.584 (br, 4H), 2.433−2.494 (m, 7H), 2.337 (s, 3H). HRMS calcd for $C_{21}H_{30}N_3O_4$ ($M + H^+$) 388.2236; found 388.2229.

4-Methyl-3-(4-methylpiperazin-1-yl)-7-(2-(piperidin-1-yl)ethoxy)-2*H*-chromen-2-one (61). Light-yellow powder in 75.8% yield. Mp 231−233 °C. ^{1}H NMR (300 MHz, DMSO-d_6): δ 7.632 (d, 1H, J = 9.0 Hz), 6.953 (br, 2H), 4.164 (br, 2H), 2.991 (br, 2H), 2.718 (br, 2H), 2.492 (br, 8H), 2.431 (s, 3H), 2.289 (s, 3H), 1.502 (br, 4H), 1.384 (m, 2H). HRMS calcd for $C_{22}H_{32}N_3O_3$ ($M + H^+$) 386.2444; found 386.2443.

4-Methyl-3-(4-methylpiperazin-1-yl)-7-(2-(pyrrolidin-1-yl)-ethoxy)-2*H*-chromen-2-one (62). Light-yellow powder in 55.0% yield. Mp 146−148 °C. ^{1}H NMR (300 MHz, DMSO-d_6): δ7.526 (d, 1H, J = 9.0 Hz), 6.820 (m, 1H), 6.610 (s, 1H), 3.603 (br, 6H), 3.335 (br, 6H), 2.779 (m, 4H), 2.523 (s, 3H), 2.392 (s, 3H). HRMS calcd for $C_{21}H_{30}N_3O_3$ ($M + H^+$) 372.2287; found 372.2289.

Biology. Materials. The CKLF1 peptide (ALIYRKLLFNPSGPYQKKPVJEKKEVL, CKLF-27) and the FITC-labeled CKLF1-27 (FITC-Acp-ALIYRKLLFNPSGPYQKKPVJEKKEVL, FITC-CKLF1-C27) with purity greater than 95% were provided by GL Biochem Ltd. (Shanghai, China). RPMI-1640 medium and fetal bovine serum (FBS) were purchased from Gibco BRL (NY). The CCR4 polyclonal antibody (rabbit anti human), p-IκB-α monoclonal antibody (ser32) (mouse anti human), IκB-α polyclonal antibody (rabbit anti human), and NFκB (P65) monoclonal antibody (rabbit anti human) were purchased from Santa Cruz Biotechnology (CA). The CKLF1 polyclonal antibody was kindly provided by Professors Dalong MA and Wenling HAN (Peking University, Beijing, China). Horseradish peroxidase-conjugated goat antirabbit IgG and FITC labeled goat antirabbit IgG were obtained from Santa Cruz Biotechnology (CA). Fluo-3/AM ester was purchased from Biotium Ltd. (CA).

Cell Culture and Transfection. HEK293 cells, obtained from American Tissue Type Collection (ATCC, MD), were grown in 75 cm^2 tissue culture flasks in RPMI-1640 medium supplemented with 10% FBS and penicillin (100 U/mL) and streptomycin (100 μg/mL) at 37 °C, 95% air−5% CO_2 in a humidified incubator.

The human pcDI-CCR4 and pcDI vector were transfected into HEK-293 cells by using Lipofactamine 2000 (Invitrogen Corp., CA) according to the manufacturer's protocol. In order to maintain CCR4 expression, 48 h later, HEK-293 cells were added with Geneticin (G418) (Invitrogen Corp., CA) at a final concentration of 500 μg/mL for the following culture. Then the monoclonal pool of stable transfected cells was selected and propagated. The expression of CCR4 was confirmed by Western blot and immunocytochemistry.

Western Blot Analysis. Cells were scraped and lysed in a lysis buffer (pH 8.0) containing 50 mM Tris-Cl, 150 mM NaCl, 1% NP-40, 1 mM PMSF, 1 mM EDTA, 1 mM DTT, 1 μg/mL aprotinin, and 1% Triton X-100 on ice. The cell lysates were solubilized in SDS sample and separated by 9% SDS−PAGE, then transferred to PVDF membrane (Millipore, MA). The membrane was blocked by 3% BSA and incubated with anti-CCR4 polyclonal antibody, followed by horseradish peroxidase (HRP)-conjugated secondary antibody, and detected with the enhanced chemiluminescence (ECL) plus detection system (LAS3000; FuJi Film Co. Ltd., Tokyo, Japan). The density of each band was quantified by using image analysis software (Science Lab 2005 Image Guage; Fuji Film Co. Ltd., Tokyo, Japan).

Immunoblot Analysis for CKLF1. Briefly, the lung tissues were lysed in buffer containing 10 mM Tris, pH 7.5, 100 mM NaCl, 1% Triton X-100, 0.1% deoxycholate, 10 μg/mL leupeptin, 100 μM phenylmethylsulfonyl fluoride, 10 μg/mL aprotinin, 5 mM EDTA, 10 mM NaF, and 2 mM Na_3VO_4 for 20 min at 4 °C. The extracts were obtained by centrifugation of lysates at 14000g for 10 min. Equal amounts of protein were analyzed by 9% SDS−PAGE and blotted onto a PVDF membrane. The membranes were blocked in 5% defatted milk powder in Tris-buffered saline for 1 h and then incubated overnight with the anti CKLF1 polyclonal antibody at 4 °C. After incubation with the peroxidase-conjugated goat anti rabbit IgG, the bands were visualized by the ECL. The density of each band was quantified by using image analysis software.

Antibodies against total NF-κB (p65), IκB-α, and phosphorylated IκB were used as indicated by the manufacturer's instructions. The total cytoplasmic protein was extracted for immunoblot according to manufacturer kits (Applygen Technologies Inc., Beijing, China). Equal amounts of protein were analyzed by 8% SDS−PAGE electrophoresis and blotted onto PVDF membrane. The membranes were blocked in 5% bovine serum albumin (antiphosphoprotein antibodies) in Tris-buffered saline for 1 h and then incubated overnight with the p-IκB-α monoclonal antibody, IκB-α polyclonal antibody, and NF-κB (P65) monoclonal antibody at 4 °C. After incubation with the peroxidase-conjugated goat antimouse IgG, goat antirabbit IgG, and goat antimouse IgG, the bands were visualized by ECL and quantified by using image analysis software.

Confocal Microscopy Analysis. The HEK293-CCR4 cells and mock-HEK293 cells were collected, coated on coverslips, and fixed with 4% paraformaldehyde for 15 min before antibody staining. Then the slides were rinsed with phosphate buffer (PBS) three times and blocked the unspecific antibody binding at room temperature with 10% normal goat serum for 1 h. The cells were incubated with 1:100 dilution of anti-CCR4 monoclonal antibody in PBS containing 5% goat serum for 2 h at room temperature, followed by incubation for 1 h with FITC-conjugated goat antirabbit IgG (1:100) at room temperature. Finally, the cells were exposed to Hoechst 33458 for 15 min after washing 3 times and the coverslips were mounted on microscope slides and the fluorescence image were obtained by confocal microscope (Leica TCS SP2, Ex = 490 nm, Em = 530 nm).

Measurements of Intracellular Calcium Flux. HEK293-CCR4 cells and mock-HEK293 cells were grown in glass-bottom microwell dishes (Corning Corporation) and loaded with 10 μM fluo-3/AM in HEPES-buffered saline at 37 °C for 1 h in the dark. The cells were rinsed with PBS and stimulated with 0.08 mM CKLF1-C27. Fluorescence was monitored at 490 nm (Ex) and 530 nm (Em) every 5 s using a Leica confocal fluorescence microscope with an ×40 oil immersion lens (Wetzler, Heidelberg, Germany) for 600 s. The measurement was completed at room temperature, and each field of cells was selected randomly. The images were analyzed for relative fluorescence using Leica confocal software. All calcium flux assays

were performed in the presence of extracellular calcium (in the absence of EDTA or EGTA) in the assay buffers. Both intracellular calcium release and extracellular calcium influx were analyzed.

Chemotaxis Activity Assay. The quantitative chemotaxis assays were performed using 24 Boyden chambers (Corning Incorporated, NY) with polyvinylpyrrolidone-free polycarbonate filters with 8 μm pores. Briefly, HEK293-CCR4 cells (1×10^6 cells/mL) were added into the upper wells (600 μL). The CKLF1-C27 with a final concentration of 100 nM was added into the lower wells. The chamber was incubated for 24 h at 37 °C in 5% CO_2 and 95% air. Cells migrating lower were counted in five randomly selected high power fields (200×) per well. HEK293 cells transfected with mock vector were used as a control. All samples were assayed three times.

Competition Binding Assay. HEK293-CCR4 cells are stable recombinant cells overexpressing the human CCR4 receptor. The cells were routinely cultured and passaged in RPMI-1640 medium. The incubators were set at 37 °C, 5% CO_2, and 95% air. HEK293-CCR4 cells were seeded into 96-well black-wall clear-bottomed polylysine coated plates (Corning Incorporated, NY), and the reaction volume was adjusted to 50 mL per well. The HEK293-CCR4 cell was planted at a density of 6×10^3 cells/well and cultured for 48 h in a 5% CO_2 humidified incubator at 37 °C. Following incubation, the supernatant was changed and the 50 μL binding buffer was added to each well. Binding buffer contained 0.08 μM FITC-CKLF1-C27, RPMI-1640, 0.5% BSA, and chemical compound. Each compound was assayed in parallel three wells. The final inhibitory value was averaged by three parallel results. The CKLF1 group only added 0.08 μM FITC-CKLF1-C27. Every group set the nonspecific control. The cells and binding buffer were then cocultured for 50 min at 37 °C. The cells were additionally rinsed with PBS gently 3 times. The fluorescence was monitored by luciferase ELIASA (BioRad, CA). The inhibition ratio (IR) was calculated using the following equation.

$$\mathrm{IR}(\%) = \frac{F_{\text{compound}} - F_{\text{compound control}}}{F_{\text{CKLF1}} - F_{\text{CKLF1 control}}}$$

F_{compound} is the fluorescence of FITC-CKLF1-C27 stimulation in the presence of compound. $F_{\text{compound control}}$ is the fluorescence in the presence of compound alone. F_{CKLF1} is the fluorescence of FITC-CKLF1-C27 stimulation alone. $F_{\text{CKLF1 control}}$ is the fluorescence in the absence of FITC-CKLF1-C27 and compound.

Histological Examination. At the end of experiment, the five mice were selected randomly from each group and sacrificed by a midline thoracotomy. Lung tissue was removed from the thorax, and the right lung was fixed by intratracheal instillation of 3 mL of 10% neutral buffered formalin. After fixation, the lungs were floated in 10% formalin for a week, embedded in paraffin, and then cut at 10 μm thickness, stained with hematoxylin−eosin and with the Masson−Goldner trichrome technique, and examined under light microscopy.

CKLF1 Induced Lung Pathological Change. The mice were anesthetized by chloral hydrate. The CKLF1 treated mice were injected with 100 μg of human CKLF1 into tibial cranial muscles. The control group was injected with 100 μg of human pCDB plasmid. At defined times after DNA injection, electroporate was performed as previously.[45] The administered group was given orally compound **41** (20 mg/kg, 120 mg/kg) daily to the human CKLF1 transfected mice. The control group was given water only. Every group was sacrificed at 3 weeks after electroporation.

Collection and Analysis of Bronchoalveolar Lavage (BAL) fluid Cells. After blood collection, tracheas were exposed by cannulating upper tracheas and BALF was collected by lavaging twice with 1 and 0.8 mL of PBS (85−90% of the input volumes were recovered). Collected lavage fluid was centrifuged at 400*g* for 5 min at 4 °C. After centrifugation, total cells were collected for differentiation.

Statistic Analysis. Data are expressed as the mean ± standard deviation (SD) as indicated. Analysis of variance (ANOVA), followed by use of sigma plot and Microsoft excel software, was performed to assess the differences between the relevant control and each experimental group. *P*-values of < 0.05 and 0.01 were regarded as statistically significant.

Acknowledgment. This work was funded by the National 863 Program of China (Grant No. 2006AA020501) and National Natural Science Foundation of China (Grant No. 90713045).

Supporting Information Available: ^{1}H and ^{13}C NMR spectra for all indicated compounds. This material is available free of charge via the Internet at http://pubs.acs.org.

References

(1) Luster, A. D. Chemokines—chemotactic cytokines that mediate inflammation. *N. Engl. J. Med.* **1998**, *338*, 436–445.
(2) Proudfoot, A. E. Chemokine receptors: multifaceted therapeutic targets. *Nat. Rev. Immunol.* **2002**, *2*, 106–115.
(3) Bazan, J. F.; Bacon, K. B.; Hardiman, G.; Wang, W.; Soo, K.; Rossi, D.; Greaves, D. R.; Zlotnik, A.; Schall, T. J. A new class of membrane-bound chemokine with a CX3C motif. *Nature* **1997**, *385*, 640–644.
(4) Zlotnik, A.; Yoshie, O. Chemokines: a new classification system and their role in immunity. *Immunity* **2000**, *12*, 121–127.
(5) Cyster, J. G. Chemokines and cell migration in secondary lymphoid organs. *Science* **1999**, *286*, 2098–2102.
(6) Luster, A. D. Chemokines—chemotactic cytokines that mediate inflammation. *N. Engl. J. Med.* **1998**, *338*, 436–445.
(7) Horuk, R. Chemokine receptors. *Cytokine Growth Factor Rev.* **2001**, *12*, 313–335.
(8) Broxmeyer, H. E. Regulation of hematopoiesis by chemokine family members. *Int. J. Hematol.* **2001**, *74*, 9–17.
(9) Youn, B. S.; Mantel, C.; Broxmeyer, H. E. Chemokines, chemokine receptors and hematopoiesis. *Immunol. Rev.* **2000**, *177*, 150–174.
(10) Mohle, R.; Bautz, F.; Denzlinger, C.; Kanz, L. Transendothelial migration of hematopoietic progenitor cells. Role of chemotactic factors. *Ann. N.Y. Acad. Sci.* **2001**, *938*, 26–34; discussion 34−35.
(11) Marra, F. Chemokines in liver inflammation and fibrosis. *Front. Biosci.* **2002**, *7*, d1899–d1914.
(12) Gillitzer, R.; Goebeler, M. Chemokines in cutaneous wound healing. *J. Leukocyte Biol.* **2001**, *69*, 513–521.
(13) De Groot, C. J.; Woodroofe, M. N. The role of chemokines and chemokine receptors in CNS inflammation. *Prog. Brain. Res.* **2001**, *132*, 533–544.
(14) Bajetto, A.; Barbero, S.; Bonavia, R.; Piccioli, P.; Pirani, P.; Florio, T.; Schettini, G. Stromal cell-derived factor-1alpha induces astrocyte proliferation through the activation of extracellular signal-regulated kinases 1/2 pathway. *J. Neurochem.* **2001**, *77*, 1226–1236.
(15) Matsui, T.; Akahoshi, T.; Namai, R.; Hashimoto, A.; Kurihara, Y.; Rana, M.; Nishimura, A.; Endo, H.; Kitasato, H.; Kawai, S.; Takagishi, K.; Kondo, H. Selective recruitment of CCR6-expressing cells by increased production of MIP-3 alpha in rheumatoid arthritis. *Clin. Exp. Immunol.* **2001**, *125*, 155–161.
(16) Yuan, G. H.; Masuko-Hongo, K.; Sakata, M.; Tsuruha, J.; Onuma, H.; Nakamura, H.; Aoki, H.; Kato, T.; Nishioka, K. The role of C-C chemokines and their receptors in osteoarthritis. *Arthritis Rheum.* **2001**, *44*, 1056–1070.
(17) Van Der Voorn, P.; Tekstra, J.; Beelen, R. H.; Tensen, C. P.; Van Der Valk, P.; De Groot, C. J. Expression of MCP-1 by reactive astrocytes in demyelinating multiple sclerosis lesions. *Am. J. Pathol.* **1999**, *154*, 45–51.
(18) Wang, G.; O, K. Homocysteine stimulates the expression of monocyte chemoattractant protein-1 receptor (CCR2) in human monocytes: possible involvement of oxygen free radicals. *Biochem. J.* **2001**, *357*, 233–240.
(19) Savarin-Vuaillat, C.; Ransohoff, R. M. Chemokines and chemokine receptors in neurological disease: raise, retain, or reduce? *Neurotherapeutics* **2007**, *4*, 590–601.
(20) Hartl, D.; Lee, C. G.; Da, S. C.; Chupp, G. L.; Elias, J. A. Novel biomarkers in asthma: chemokines and Chitinase-like proteins. *Curr. Opin. Allergy Clin. Immunol.* **2009**, *9*, 60–66.
(21) Barnes, P. J. New drugs for asthma. *Nat. Rev. Drug Discovery* **2004**, *3*, 831–844.

(22) Han, W.; Ding, P.; Xu, M.; Wang, L.; Rui, M.; Shi, S.; Liu, Y.; Zheng, Y.; Chen, Y.; Yang, T.; Ma, D. Identification of eight genes encoding chemokine-like factor superfamily members 1−8 (CKLFSF1−8) by in silico cloning and experimental validation. *Genomics* **2003**, *81*, 609–617.
(23) Han, W.; Lou, Y.; Tang, J.; Zhang, Y.; Chen, Y.; Li, Y.; Gu, W.; Huang, J.; Gui, L.; Tang, Y.; Li, F.; Song, Q.; Di, C.; Wang, L.; Shi, Q.; Sun, R.; Xia, D.; Rui, M.; Tang, J.; Ma, D. Molecular cloning and characterization of chemokine-like factor 1 (CKLF1), a novel human cytokine with unique structure and potential chemotactic activity. *Biochem. J.* **2001**, *357*, 127–135.
(24) Zhong, W.; Zeng, G.; Cai, Y.; Tan, Y.; Hen, S.; Dai, Q.; He, H.; Hu, J.; Wei, H. Pathological changes in seminiferous tubules in infertility rats induced by chemokine-like factor I. *Chin. J. Exp. Surg.* **2003**, *20*, 1027–1028.
(25) Li, T.; Zhong, J.; Chen, Y.; Qiu, X.; Zhang, T.; Ma, D.; Han, W. Expression of chemokine-like factor 1 is upregulated during T lymphocyte activation. *Life Sci.* **2006**, *79*, 519–524.
(26) Tan, Y. X.; Han, W. L.; Chen, Y. Y.; Ouyang, N. T.; Tang, Y.; Li, F.; Ding, P. G.; Ren, X. L.; Zeng, G. Q.; Ding, J.; Zhu, T.; Ma, D. L.; Zhong, N. S. Chemokine-like factor 1, a novel cytokine, contributes to airway damage, remodeling and pulmonary fibrosis. *Chin. Med. J.* (*Engl.*) **2004**, *117*, 1123–1129.
(27) Wang, Y.; Zhang, Y.; Yang, X.; Han, W.; Liu, Y.; Xu, Q.; Zhao, R.; Di, C.; Song, Q.; Ma, D. Chemokine-like factor 1 is a functional ligand for CC chemokine receptor 4 (CCR4). *Life Sci.* **2006**, *78*, 614–621.
(28) Wang, Y.; Zhang, Y.; Han, W.; Li, D.; Tian, L.; Yin, C.; Ma, D. Two C-terminal peptides of human CKLF1 interact with the chemokine receptor CCR4. *Int. J. Biochem. Cell Biol.* **2008**, *40*, 909–919.
(29) Sallusto, F.; Lenig, D.; Mackay, C. R.; Lanzavecchia, A. Flexible programs of chemokine receptor expression on human polarized T helper 1 and 2 lymphocytes. *J. Exp. Med.* **1998**, *187*, 875–883.
(30) Bonecchi, R.; Bianchi, G.; Bordignon, P. P.; D'Ambrosio, D.; Lang, R.; Borsatti, A.; Sozzani, S.; Allavena, P.; Gray, P. A.; Mantovani, A.; Sinigaglia, F. Differential expression of chemokine receptors and chemotactic responsiveness of type 1 T helper cells (Th1s) and Th2s. *J. Exp. Med.* **1998**, *187*, 129–134.
(31) D'Ambrosio, D.; Iellem, A.; Bonecchi, R.; Mazzeo, D.; Sozzani, S.; Mantovani, A.; Sinigaglia, F. Selective up-regulation of chemokine receptors CCR4 and CCR8 upon activation of polarized human type 2 Th cells. *J. Immunol.* **1998**, *161*, 5111–5115.
(32) Banwell, M. E.; Robinson, D. S.; Lloyd, C. M. Adenoid-derived TH2 cells reactive to allergen and recall antigen express CC chemokine receptor 4. *J. Allergy Clin. Immunol.* **2003**, *112*, 1155–1161.
(33) Zhou, L. F.; Zhang, M. S.; Yin, K. S.; Ji, Y; Xie, W. P.; Cui, X. F.; Ji, X. H. Effects of adenoviral gene transfer of mutated IκBα, a novel inhibitor of NF-κB, on human monocyte-derived dendritic cells. *Acta Pharmacol. Sin.* **2006**, *27*, 609–616.
(34) Trautmann, A.; Schmid-Grendelmeier, P.; Kruger, K.; Crameri, R.; Akdis, M.; Akkaya, A.; Brocker, E. B.; Blaser, K.; Akdis, C. A. T cells and eosinophils cooperate in the induction of bronchial epithelial cell apoptosis in asthma. *J. Allergy Clin. Immunol.* **2002**, *109*, 329–337.
(35) Fujihara, S.; Ward, C.; Dransfield, I.; Hay, R. T.; Uings, I. J.; Hayes, B.; Farrow, S. N.; Haslett, C.; Rossi, A. G. Inhibition of nuclear factor-kappaB activation un-masks the ability of TNF-alpha to induce human eosinophil apoptosis. *Eur. J. Immunol.* **2002**, *32*, 457–466.
(36) Ghosh, S.; May, M. J.; Kopp, E. B. NF-kappa B and Rel proteins: evolutionarily conserved mediators of immune responses. *Annu. Rev. Immunol.* **1998**, *16*, 225–260.
(37) Papavassiliou, A. G. Molecular medicine. Transcription factors. *N. Engl. J. Med.* **1995**, *332*, 45–47.
(38) Kopp, E. B.; Ghosh, S. NF-kappa B and rel proteins in innate immunity. *Adv. Immunol.* **1995**, *58*, 1–27.
(39) Hart, L; Lim, S; Adcock, I; Barnes, P. J.; Chung, K. F. Effects of inhaled corticosteroid therapy on expression and DNA-binding activity of nuclear factor κB in asthma. *Am. J. Respir. Crit. Care Med.* **2000**, *161*, 224–231.
(40) Barnes, P. J.; Karin, M. Nuclear factor-kappaB: a pivotal transcription factor in chronic inflammatory diseases. *N. Engl. J. Med.* **1997**, *336*, 1066–1071.
(41) Baeuerle, P. A.; Baltimore, D. NF-kappa B: ten years after. *Cell* **1996**, *87*, 13–20.
(42) Baldwin, A. S., Jr. The NF-kappa B and I kappa B proteins: new discoveries and insights. *Annu. Rev. Immunol.* **1996**, *14*, 649–683.
(43) (a) Zhang, L.; Liu, G.; Zhang, S. D.; Yang, H. Z.; Li, L.; Wu, X. H.; Yu, J. L.; Kou, B. B.; Xu, S.; Li, J.; Sun, G. C.; Ji, Y. F.; Cheng, G. F. Parallel approach for solution-phase synthesis of 2-quinoxalinol analogues and their inhibition of LPS-induced TNF-α release on mouse macrophages in vitro. *J. Comb. Chem.* **2004**, *6*, 431–436. (b) Li, L.; Liu, G.; Wang, Z. G.; Yuan, Y. Y.; Zhang, C. X.; Tian, H. Y.; Wu, X. H.; Zhang, J. Multistep parallel synthesis of substituted 5-aminobenzimidazoles in solution phase. *J. Comb. Chem.* **2004**, *6*, 811–821. (c) Zhang, J.; Zhang, L.; Zhang, S. D.; Wang, Y. H.; Liu, G. Solution-phase parallel synthesis of a 1,2,7-trialkyl-1H-imidazo[4,5-g]quinoxalin-6-ol library scaffold. *J. Comb. Chem.* **2005**, *7*, 657–664. (d) Yang, T. M.; Liu, G. Solution-phase parallel synthesis of 3,5,6-substituted indolin-2-ones. *J. Comb. Chem.* **2007**, *9*, 86–95. (e) Yuan, Y. Y.; Liu, G.; Li, L.; Wang, Z. G.; Wang, L. Synthesis of diverse benzo[1,4]oxazin-3-one-based compounds using 1,5-difluoro-2,4-dinitrobenzene. *J. Comb. Chem.* **2007**, *9*, 158–170. (f) Wang, Z. G.; Yuan, Y. Y.; Chen, Y. Y.; Sun, G. C.; Wu, X. H.; Zhang, S. M.; Han, C. Y.; Wang, G. X.; Li, L.; Liu, G. Parallel solution-phase synthesis of 4H-benzo[1,4]thiazin-3-one and 1,1-dioxo-1,4-dihydro-2H-1λ^6-benzo[1,4]thiazin-3-one derivatives from 1,5-difluoro -2,4-dinitrobenzene. *J. Comb. Chem.* **2007**, *9*, 652–660. (g) Zhao, H. Y.; Liu, G. Solution-phase parallel synthesis of 2,3-dihydro-1,5-benzothiazepin-4(5H)-ones. *J. Comb. Chem.* **2007**, *9*, 756–772. (h) Zhao, H. Y.; Liu, G. Solution-phase parallel synthesis of diverse 1,5-benzodiazepin-2-ones. *J. Comb. Chem.* **2007**, *9*, 1164–1176. (i) Liu, G.; Li, L.; Kou, B. B.; Zhang, S. D.; Zhang, L.; Yuan, Y. Y.; Ma, T.; Shang, Y.; Li, Y. C. Benzofused tricycles based on 2-quinoxalinol. *J. Comb. Chem.* **2007**, *9*, 70–78.
(44) Neelakantan, S.; Raman, P. V.; Tinabaye, A. A new and convenient synthesis of 4-methyl-3-phenyl-coumarins and 3-phenylcoumarin. *Indian J. Chem.* **1982**, *21B*, 256–257.
(45) Mir, L. M.; Bureau, M. F.; Gehl, J.; Rangara, R.; Rouy, D.; Caillaud, J. M.; Delaere, P.; Branellec, D.; Schwartz, B.; Scherman, D. High-efficiency gene transfer into skeletal muscle mediated by electric pulses. *Proc. Natl. Acad. Sci. U.S.A.* **1999**, *96*, 4262–4267.